UNIVERSITÉ LIBRE DE BRUXELLES

BRUFACE BRUSSELS FACULTY OF ENGINEERING

VRIJE UNIVERSITEIT BRUSSEL

Graduation thesis submitted in partial fulfilment of the requirements for the degree of engineering sciences: Chemical and Materials Engineering

Experimental study of the diffusion coefficient of high-voltage LNMO spinel positive electrodes for next-generation Li-ion batteries

Manon Winnock

Master thesis submitted under the supervision of
Prof. Annick Hubin

The co-supervision of
Dr. Xinhua Zhu

The advice of
Joan Roca Busacker

Master's thesis submitted in order to be awarded the Master's Degree in
Chemical and Materials Engineering: Profile Materials

Academic year
2023-2024

Abstract

"Experimental study of the diffusion coefficient of high-voltage LNMO spinel positive electrodes for next-generation Li-ion batteries"

Manon Winnock

Master of Chemical and Materials Engineering: Profile Materials

Academic year: 2023-2024

Lithium-ion batteries play an important role in the global shift away from traditional fossil fuel technologies toward more sustainable energy production and storage solutions. However, with increasing demand for Li-ion batteries, the reliance on critical raw materials, under which cobalt, escalates as well. One potential solution lies in developing cobalt-free electrodes, which could mitigate dependency on scarce resources. This master's thesis focuses on studying next-generation high-voltage $LiNi_{0.5}Mn_{1.5}O_4$ (LNMO) spinel positive electrode materials. To model the optimal design of Li-ion batteries containing this LNMO positive electrode, it is important to obtain reliable and quantitative values for among others the lithium ion diffusion coefficient. Lithium diffusion within electrodes plays a crucial role in determining the battery's charge/discharge rates. So, the main objective of this thesis is to establish a robust understanding of the evolution of the lithium diffusion coefficient in thin film LNMO electrodes through diverse experimental approaches. The electrode being a thin film instead of a composite allows to model a system where other components such as binders and conductive additives are avoided. The techniques used to determine the diffusion coefficient are the Galvanostatic Intermittent Titration Technique (GITT), the Potentiostatic Intermittent Titration Technique (PITT) and Intermittent Current Interruption (ICI). With these techniques the evolution of the diffusion coefficient as a function of potential can be determined. The three techniques result in diffusivities that differ in order of magnitude, but show the same trends. For ICI, PITT and GITT respectively diffusion coefficients varying from 10^{-9} to 10^{-13} cm^2/s, 10^{-11} to 10^{-13} cm^2/s and 10^{-13} to 10^{-15} cm^2/s are found. By comparing the different techniques, PITT is found to be the most reliable to determine the diffusion coefficient for thin film LNMO electrodes, especially in the high-voltage window. Furthermore, the impact of the thin film electrode thickness is explored as well. This showed a change in behaviour starting from a thickness of 200 nm.

Keywords: $LiNi_{0.5}Mn_{1.5}O_4$, thin film, diffusion coefficient, GITT, PITT, ICI

Acknowledgements

First, I would like to thank my supervisor Prof. Annick Hubin and co-supervisor Dr. Xinhua Zhu for the opportunity to work on this project and their feedback along the way. I would also like to express my gratitude towards my advisor Joan Busacker for his guidance, support and advice. Being able to discuss my results with him was of great help.

Furthermore, I would like to thank the people of the SURF department for creating such a nice working environment.

I would also like to thank my parents for their support and encouragement from the beginning of my education.

Finally, I would like to thank my friends for creating all of these happy memories throughout these five years.

Thank you everyone,
Manon

Contents

Chapter 1

Introduction and objectives

Lithium-ion batteries have become an integral part of modern life, powering a vast array of portable electronic devices including cellular phones, laptops, and digital cameras. Beyond consumer electronics, these batteries are increasingly vital in the global shift away from traditional fossil fuel technologies toward more sustainable energy production and storage solutions. They play a pivotal role in the adoption of electric vehicles and the integration of renewable energy sources into power grids.

However, as the demand for lithium-ion batteries escalates, so does our reliance on critical raw materials, notably lithium and cobalt. Securing these resources is proving to be a growing challenge with potentially significant environmental consequences. Cobalt, in particular, holds exceptional value as a key component of lithium-ion battery positive electrodes. Forecasts indicate potential deficits in cobalt supply as early as 2030, highlighting the urgency to address this issue. Moreover, the majority of cobalt production is concentrated in the Democratic Republic of the Congo, where mining operations often involve unethical practices and face geopolitical instability, further underscoring the need for alternative battery systems.

One potential solution lies in developing cobalt-free electrodes, which could mitigate dependency on scarce resources. However, current commercial batteries utilizing these materials do not yet match the performance standards—specifically in terms of cyclability, durability, and efficiency—set by cobalt-containing counterparts. Consequently, further research and development efforts are crucial to enhance the competitiveness of alternative battery technologies.

This master's thesis focuses on advancing the understanding of next-generation high-voltage $LiNi_{0.5}Mn_{1.5}O_4$ (LNMO) spinel positive electrode materials. To optimize lithium-ion batteries, investigating the kinetic parameters governing lithium intercalation electrodes is essential. Lithium diffusion within the electrodes plays a critical role in determining the battery's charge/discharge rates. This thesis will determine the lithium diffusion coefficient in LNMO positive electrode thin films, also taking into account how electrode thickness influences the electrochemical behaviour. The evolution of the diffusion coefficient during charging will be studied using various experimental techniques, including the Galvanostatic Intermittent Titration Technique, the Potentiostatic Intermittent Titration Technique, and Intermittent Current Interruption. These methods apply transient current or potential and measure the corresponding potential or current response, enabling a comprehensive analysis of lithium diffusion behaviour in LNMO electrodes.

The primary objective of this master's thesis is to establish a robust understanding of the evolution of the lithium diffusion coefficient in LNMO electrodes through diverse experimen-

tal approaches. Therefore, different methods need to be developed to determine the diffusion coefficient. Additionally, this research will explore the impact of electrode thickness on its electrochemical behaviour, providing valuable insights to advance lithium-ion battery technology and contribute to the development of more efficient and sustainable energy storage solutions.

Chapter 2

State of the art

2.1 Energy

On 15 November 2022 the world's population reached 8 billion people, which is three times more than in the mid-twentieth century ("Population", n.d.). With increasing human population, the consumption of natural resources rises as well. The development of science and technology in the 19^{th} century created many improvements in society standards and quality of life. However, it also came with a cost. It launched an unsustainable cycle of economic growth that caused dependence on scarce materials and a global climate change resulting in extreme weather conditions mostly impacting vulnerable communities (Intergovernmental Panel on Climate Change, 2023). The global climate change manifests itself under a global surface temperature that is 1.1°C higher in 2011-2020 compared to 1850-1900. The rise in temperature can mainly be attributed to the continued increase in emissions of greenhouse gasses (GHG). The global greenhouse gas emission by economic sectors is given in Figure 2.1. The largest share and growth in GHG emissions occurs under the form of CO_2 from fossil fuel combustion and industrial processes (Intergovernmental Panel on Climate Change, 2023).

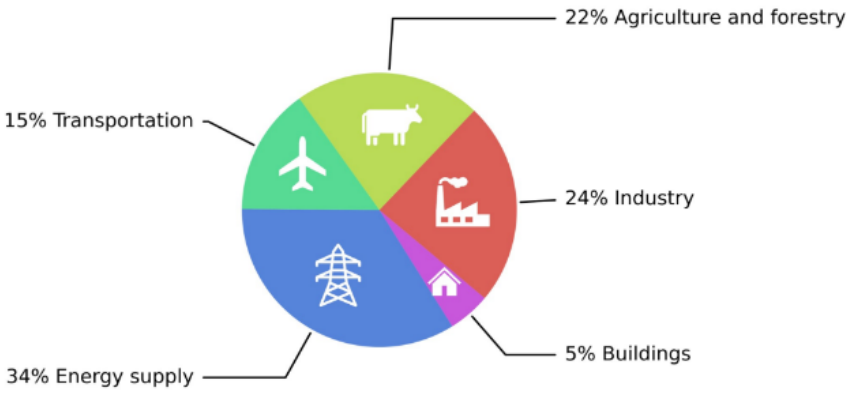

Figure 2.1: Global GHG emission by economic sector. The energy supply sector corresponds to heat and electricity production, and the building sector comprises onsite energy generation and burning fuels for commercial and private households heating (Intergovernmental Panel on Climate Change, 2023; Soult, 2023).

Limiting human-caused global warming requires net zero CO_2 emissions. Until this is reached, the reduction in cumulative carbon and GHG emissions this decade will largely determine whether warming can be limited to 1.5 °C or 2 °C. For the energy supply sector a radical shift from a model dependent on fossil fuels to a system based on renewable energy sources and reduced production and consumption, is required to tackle this issue (Intergovernmental Panel on Climate Change, 2023). Renewable energy sources (such as solar or wind energy) require energy storage. For these systems, aspects such as the rate of energy storage, long service life (number of cycles) and a relatively low cost are very important (Kulova et al., 2020). Energy can be stored in many ways, for example as compressed air that is afterwards decompressed in a turbine running a generator (De Decker, 2020; Vieira et al., 2021), as kinetic energy in a flywheel (Amiryar & Pullen, 2017), as chemical energy in hydrogen liquid or gas (Hirscher et al., 2020), or as chemical energy in an electrochemical battery. Currently, lithium-ion batteries (LIB) are beginning to dominate the field with a high energy density, a high power density and a prolonged lifetime when compared to other battery types (Kulova et al., 2020; Soult, 2023).

However, the popularity of LIB has raised the dependence on scarce materials, such as lithium and cobalt. The most important Lithium-production sites are in South America (Chile and Argentina) and in Australia. Accessing these resources will become more difficult with higher impacts on the environment. Even with these larger efforts and with recycling of lithium, the long-term availability of lithium might still be insufficient for the growing demand (Wanger, 2011). On the other hand, cobalt is present in the positive electrode. Cobalt is the most valuable component in LIB and deficits in cobalt supply could occur as early as 2030. Cobalt is considered a critical resource as around 60% of the worldwide mine production in 2018 originated from copper-cobalt ores in the Democratic Republic of the Congo (DRC). Here, cobalt is being mined under unethical working conditions and geopolitical instability. Moreover, Chinese companies dominate most of the cobalt mining operations in the DRC. Considering that China might experience cobalt supply deficits itself by 2030, China's cobalt production will likely prioritize domestic battery manufacturers (Gourley et al., 2020). The upcoming cobalt supply deficits and unpredictable market prices of raw cobalt make the need for cobalt-free energy storage solutions clear.

2.2 Batteries

A battery can store chemical energy and convert it into electrical energy during charge and discharge (Winter & Brodd, 2004). Inside a battery, electrochemical processes occur. These are chemical reactions where electrons are transferred, via an external circuit, to or from a chemical species, producing a change in its oxidation state. The general reaction in every electrochemical process is (Soult, 2023):

$$\mathrm{Ox} + \mathrm{ne}^- \rightleftharpoons \mathrm{Red}$$

With:

- Ox = oxidized species
- Red = reduced species
- n = number of electrons transferred during the reaction

Each battery consists of multiple electrochemical cells that are electrically connected, with contacts to supply electrical energy. With these contacts electrons are collected and flow through an external circuit, while ions flow between two electrodes through the electrolyte inside each

electrochemical cell. The two electrodes are the cathode and the anode, where respectively the reduction and oxidation reaction take place (Winter & Brodd, 2004). In Figure 2.2, a representation of an electrochemical cell is given.

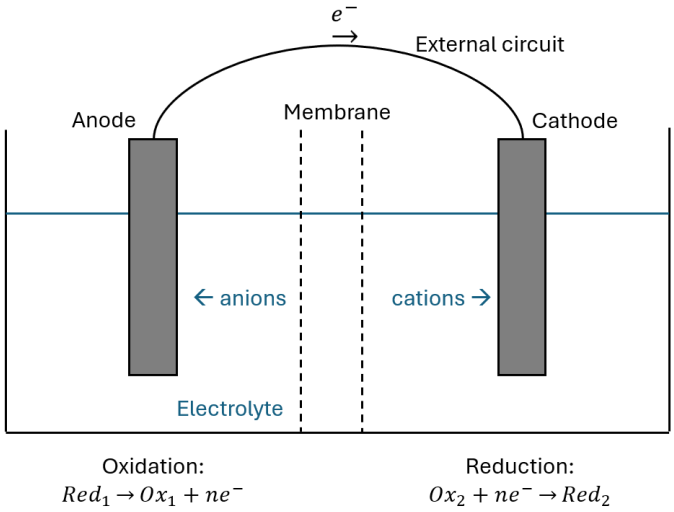

Figure 2.2: The representation of an electrochemical cell.

In a battery the electrodes are also referred to as the positive and the negative electrode. Depending on whether the battery is in charge or discharge mode their roles will be different. During discharge the positive electrode is the cathode and the negative electrode is the anode. During charge it is the other way around. This is represented in Table 2.1. In this work LNMO is the cathode in discharge mode, it will be referred to as the positive electrode.

Table 2.1: The link between the positive and negative electrode on the one hand and the cathode and anode on the other hand.

Electrode	**Discharge**	**Charge**
Positive electrode	Cathode	Anode
Negative electrode	Anode	Cathode

Some basic terms to be able to compare and evaluate different batteries are:

- Capacity

  The capacity is the amount of electrical energy a battery can deliver under specific discharge conditions (Rubenbauer & Henninger, 2017). It is defined in units of Ah. In simpler terms, the capacity of a battery gives an idea of how long a battery can power a device before it needs to be recharged. For example, a battery with a capacity of 3 Ah can theoretically deliver a current of 3 A for 1 hour, 1.5 A for two hours and so on (Aktaş & Kirçiçek, 2021). When referring to the capacity of an electrode, it needs to be normalized with respect to the active mass or volume in active mass[1] in the electrode. These are defined in units of respectively Ah/kg and Ah/cm^3 (Soult, 2023).

[1]The active mass is the material that generates electrical current with a chemical reaction within the battery (Winter & Brodd, 2004).

- Power

  The power of a battery indicates how quickly a battery can deliver energy to a system. Higher power batteries can supply energy more quickly, which is important for applications where a high power output is required, such as powering electric vehicles (Saft, n.d.). The power of a battery is given by the product of the current and voltage during charge or discharge. It is expressed in W (Korthauer, 2018).

- Energy

  The energy of a battery refers to the total amount of energy it can store and deliver. It represents the total amount of work that can be done by the battery when it is discharged (Saft, n.d.). The energy of a battery is given by the product of the capacity and the average discharge voltage. It is expressed in Wh (Korthauer, 2018). The specific energy is normalized by the mass of the full battery and expressed in Wh/kg. On the other hand the energy density is normalized by the volume of the battery and expressed in Wh/cm^3 (Winter & Brodd, 2004).

- C-rate

  The C-rate is a measure of the rate at which the battery is charged or discharged relative to its maximum capacity. A 1C rate means the battery is being charged or discharged for one hour at a current equal to its capacity. For example a battery with a capacity of 100 Ah has a 1C rate equal to 100 A. This means the battery is completely discharged in one hour when the discharge current is equal to 100 A. A 5C rate for this battery would equate to a discharge current of 500 A and a C/2 rate to a discharge current of 50 A. So, in summary the C-rate helps to understand how quickly a battery is being charged or discharged (MIT Electric Vehicle Team, 2008).

The difference between energy and power is visualized in Figure 2.3. The larger the bottle or cup, the more water it can hold. This is comparable to a battery's energy. The opening through wich the water is poured determines how fast it can be poured. This is similar to a battery's power (Saft, n.d.).

Figure 2.3: The mug has a high power density since it can empty all of its content almost simultaneously. The jug, on the other hand releases its content more slowly, but holds more water (more "energy") than the mug (Energy Education, n.d.; Tecate Group, n.d.).

A battery has some important properties. Its voltage should be constant and with a minimum overpotential. The overpotential is the extra potential needed (with respect to the reversible

reaction potential) to overcome the activation barrier and allow the reaction to occur (Brett & Brett, 1993). Furthermore, on discharging the battery, the voltage should remain constant as well. While storing the battery, self-discharge should be limited (Hubin, 2021). Self-discharge is a spontaneous loss of energy from a charged storage device without connecting to the external circuit. This energy loss can be caused by multiple mechanisms that shift the storage system from a higher-charged free energy state to a lower free state. A few examples are: side reactions at the electrode surfaces, presence of impurities in low concentrations, leakage current,... (Babu, 2024).

2.3 Lithium-ion batteries

Lithium is considered an important metal available for battery chemistry. Apart from being non-toxic, it is very light and has a redox potential of -3.05 V with respect to the standard hydrogen electrode (SHE) which is very low. This fundamental advantage over other chemistries allows lithium-based batteries to have a higher potential for energy storage (Korthauer, 2018; Zubi et al., 2018). However, as a result of this redox potential lithium is also very reactive, which makes it technologically challenging to build safe battery cells containing metallic lithium. Another problem with metallic lithium as electrode is the risk of dendritic growth during charging causing short circuits. Therefore, intercalation compounds capable of donating lithium ions are used rather than metallic lithium (Megahed & Scrosati, 1994). As a result of their small size, lithium ions are able to intercalate inside the positive and negative electrode materials. They are the charge carriers in the electrolyte and act as counter-charge to compensate for the external current flow.

Since the negative electrode material is employed in unlithiated form (the lithium-ion battery is assembled uncharged), the positive electrode material has to contain the necessary lithium (Korthauer, 2018).

2.3.1 Mechanism

Figure 2.4 represents the schematic of a rechargeable lithium-ion battery. Single lithium ions migrate back and forth between the positive and the negative electrode, through an electrolyte and a separator during charging and discharging. The electrolyte contains a dissociated lithium conducting salt. The separator is a porous membrane that electrically isolates the two electrodes, but allows the passing of lithium-ions. During discharging, lithium is deintercalated from the negative electrode (in the case of discharging this is the anode) and electrons are released. The lithium ions then migrate towards the positive electrode (in the case of discharging this is the cathode). At the same time electrons flow from the negative to the positive electrode via an external connection. During charging the process is reversed. Lithium ions migrate from the positive (now the anode) to the negative electrode (now the cathode) (Hausbrand et al., 2015; Korthauer, 2018).

2.3.2 The first commercial lithium-ion battery

The first commercial lithium-ion battery consisted of a negative electrode made from graphite, a positive electrode made from $LiCoO_2$ and an electrolyte[2] made of organic carbonates and lithium hexafluorophosphate ($LiPF_6$). It has an average voltage of around 3.6 V. $LiCoO_2$ has a layered

[2]The electrolyte cannot be aqueous because of the high reducing power of lithium. It must be based on organic solvents.

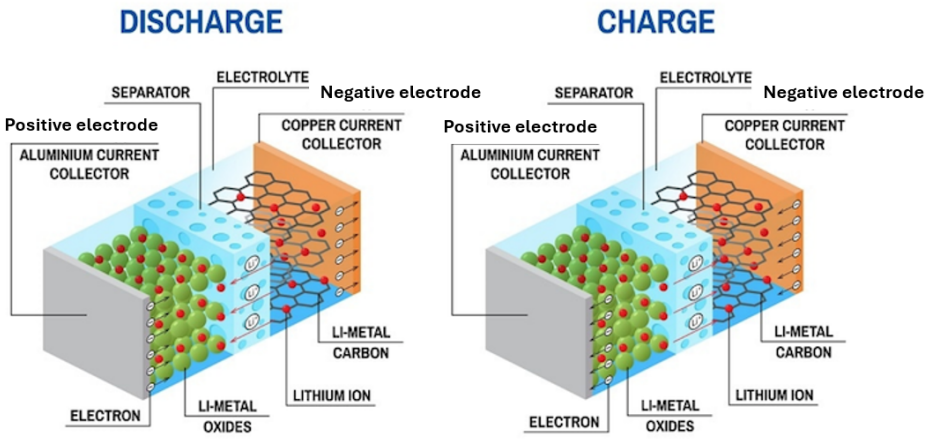

$$C_6 + LiMO_2 \underset{Discharge}{\overset{Charge}{\rightleftarrows}} Li_xC_6 + Li_{(1-x)}MO_2$$

Figure 2.4: The schematic of a lithium-ion battery (with M standing for metal) (EV Express, n.d.).

structure with alternating cobalt, oxygen and lithium-ion layers. For complete discharging the reaction taking place at the positive electrode is (Korthauer, 2018):

$$2Li_{0.5}CoO_2 + Li^+ + e^- \rightarrow 2LiCoO_2$$

The traditional negative electrode is made from graphitic carbon. This material has carbon atoms in parallel graphene layers. Unlike cobalt dioxide, graphite is stable without lithium, which means it can be almost completely discharged. For complete discharging the reaction at the negative electrode is (Korthauer, 2018; Megahed & Scrosati, 1994):

$$LiC_6 \rightarrow Li^+ + e^- + 6C$$

2.3.3 Applications

Each electric energy storage (EES) technology has its own performance characteristics that make it more or less suitable for a specific application. These key properties are among others: energy density, specific energy, specific power, self-discharge rate, full charge and discharge times, initial cost and safety. Next to that, some EES systems are adaptable to mobile applications while others are strictly stationary. Furthermore, some technologies can be produced as small size units, while others can not. In Figure 2.5 a comparison of specific energy and power for different EES technologies is given. From this figure it becomes clear that LIB have a high specific power and energy compared to other commercial batteries (Zubi et al., 2018).

As specific energy and power are key criteria in portable electronic applications (such as cellular phones, laptops, digital cameras, video games,...) the Li-ion battery has a clear advantage over other chemistries. Portable electronics have been the initial market for LIB (Naskar et al., 2023; Zubi et al., 2018). Besides portable electronics, today's market in (hybrid) electric vehicles is also dominated by LIB. The high voltage, high energy density, high specific energy and

rechargeable ability make LIBs the preferred energy source for (hybrid) electric vehicles (Chen et al., 2023; Zubi et al., 2018). Lastly, Li-ion batteries are also of significance in power supply systems. These systems include both grid- and off-grid systems. In the electricity grid supply and demand of power have to be balanced, however, both of them are variable. The electricity demand can vary along the day, but also along different seasons. On the other side, the power supply can vary as some technologies do not have a constant output, such as photovoltaic (PV) and wind power. The electricity grid has thus relied on energy storage units for support in adapting supply and demand and providing ancillary services. Next to that, there is an increasing degree of decentralization with consumers becoming prosumers by installing their own power generation units, such as rooftop PV systems. This is making electrochemical storage solutions, including LIB, more and more important. Durable and low-cost variants of Li-ion batteries are used in large-scale energy storage applications. An example of such a variant are batteries with carbon-coated $LiFePO_4$ positive active material. These batteries effectively store renewable energy for green electricity and grid energy for power backup (Naskar et al., 2023; Zubi et al., 2018).

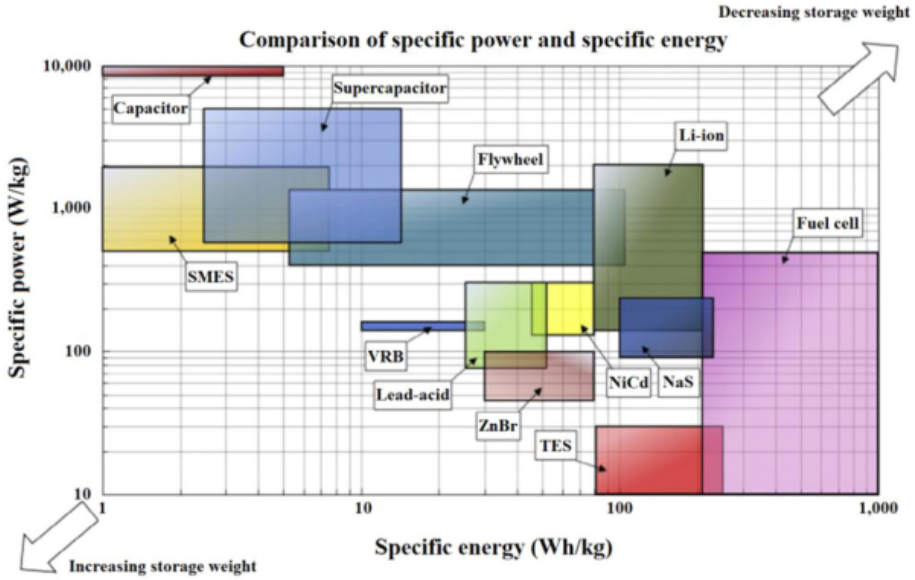

Figure 2.5: Comparison of the specific energy and power for different EES technologies. Acronyms: SMES (superconducting magnetic energy storage), VRB (vanadium redoc battery), NaS (sodium-sulphur), TES (thermal energy storage) (Zubi et al., 2018).

2.4 Transition metal oxides for the positive electrode

For the traditional lithium-ion battery the main challenges are safety, cost and size. As more and more larger batteries are built for electric vehicles and other large-scale applications, the importance of safety and cost has become increasingly significant. This is because in case of failure the consequences become larger and in order to compete with for example gasoline tanks a battery pack for a full-electric car cannot be too expensive (Korthauer, 2018).

The need for cobalt-free positive electrodes becomes clear when looking at the upcoming cobalt supply deficits, unpredictable market prices, unethical mining and toxicity. The first

cobalt-free commercial positive electrode was the olivine $LiFePO_4$ (LFP) positive electrode. LFP has a high thermal stability, excellent cycle life, a flat charge/discharge profile and a high electrochemical stability over more or less 100% depth of discharge. However, it has a low energy density and nominal voltage (around 3.3 V vs. graphite negative electrode) because of which it achieved little market traction in Western markets (Gourley et al., 2020). Another cobalt-free positive electrode is spinel $LiMn_2O_4$ (LMO). The host structure allows 3D solid-state diffusion of lithium-ions, which results in high LIB rate performances. However, because of the presence of Mn^{3+} it only has a low practical capacity and cycle stability. The electronic configuration of Mn^{3+} induces Jahn-Teller distortion. This can cause lattice changes from the cubic to tetragonal phase which constricts Li^+ diffusion. Next to that, Mn^{3+} (solid) can undergo a disproportionation reaction forming Mn^{4+} (solid) and Mn^{2+} (solution). Mn^{2+} dissolves in the electrolyte, which means there is a capacity fade over time (Gourley et al., 2020).

Suppression of Jahn-Teller distortion has commonly been addressed by partially substituting Mn with other cations to reduce the amount of Mn^{3+} (Gourley et al., 2020). Transition-metal-substituted spinel materials with a general formula of $LiM_xMn_{2-x}O_4$ (with M = Cr, Co, Fe, Ni, Cu) have emerged. Among those materials, the high voltage lithium containing nickel-based oxide positive electrode, $LiNi_{0.5}Mn_{1.5}O_4$ (LNMO), where part of the manganese is substituted by nickel is of special interest (Amin et al., 2020; Kim et al., 2004). This is because of its high discharge capacity and dominant plateau at around 4.7 V, while other materials show two plateaus at around 4.0 and 5 V (Kim et al., 2004).

2.4.1 Properties of LNMO

The $LiNi_{0.5}Mn_{1.5}O_4$ spinel positive electrode has a theoretical capacity[3] of 146.7 mAh/g. This results from the intercalation of one lithium-ion per formula unit through a corresponding oxidation of Ni^{2+} to Ni^{4+}. Furthermore, LNMO operates at high voltages, more specifically 4.70 - 4.75 V vs. Li/Li^+, at very high charging and discharging rates. This high discharge voltage leads to a high energy density of around 690 Wh/kg, which is 20% higher than for $LiCoO_2$ and 30% higher than for $LiFePO_4$ when employed as positive electrode against a graphitic negative electrode (Amin et al., 2020; Bhatia et al., 2021). Because of its robust 3D spinel lattice structure (which enables fast movement of Li^+ ions), LNMO is also considered for extremely fast charging applications. All these factors make $LiNi_{0.5}Mn_{1.5}O_4$ an attractive candidate for safe, energy-dense and high-power applications. These applications go from portable electronics and grid energy storage to enabling intermittent renewables through both centralized and decentralized infrastructures (Amin et al., 2020).

However, the high potential of LNMO positive electrodes is also a critical issue. It leads to electrolyte decomposition and concurrent degradation reactions, which results in rapid capacity fade (Bhatia et al., 2021).

2.4.2 Reaction taking place

During delithiation Ni^{2+} is oxidized to Ni^{4+} via the Ni^{3+} state. This is expressed in the electrochemical reaction below (Rahim et al., 2022):

$$\begin{aligned} &\mathrm{LiNi(II)_{0.5}Mn(IV)_{1.5}O_4} \\ &\rightarrow \mathrm{Li_{0.5}Ni(III)_{0.5}Mn(IV)_{1.5}O_4} + 0.5\mathrm{Li^+} + 0.5\mathrm{e^-} \\ &\rightarrow \mathrm{Ni(IV)_{0.5}Mn(IV)_{1.5}O_4} + 0.5\mathrm{Li^+} + 0.5\mathrm{e^-} \end{aligned}$$

[3]Theoretical capacity = (nF/(3600*M_w)), where n = 1, F = 96485 C/mol and M_w = 189.6 g/mol

In the low potential window, the present Mn^{3+} is also oxidized to Mn^{4+} during delithiation.

2.4.3 Structure of LNMO

Many lithium-ion battery positive electrode materials have a layered structure which enables two-dimensional diffusion of the lithium ions, or a spinel structure, enabling three-dimensional diffusion (Yoshio et al., 2009). The third positive electrode class are the polyanion oxides, of which the best-known is the polyanionic olivine $LiMPO_4$ (M = Fe, Mn, Co or Ni) (Mohamed & Allam, 2020). An example of a layered structure is $LiCoO_2$, in which Li^+ and Co^{3+} ions are ordered on alternate (111) planes in a rock salt structure[4] with a cubic close-packed array of oxide ions, as can be seen in Figure 2.6. The large difference in size and charge between Li^+ and Co^{3+} leads to good cation ordering. This is important for fast two-dimensional lithium-ion diffusion and conductivity in the lithium plane (Manthiram, 2020).

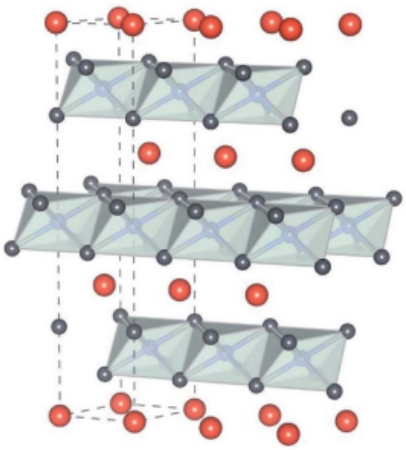

Figure 2.6: The crystallographic framework of layered $LiCoO_2$ consisting of CoO_6 octahedra (grey) and Li^+ (orange) (Mohamed & Allam, 2020).

Spinel LNMO has a robust cubic close-packed crystal structure made of edge-sharing MO_6 octahedra (with M = Mn or Ni) with six equal Mn/Ni-O distances. Whereas, lithium is tetrahedrally coordinated with four oxygen atoms in four equal Li-O distances. The edge-sharing octahedra share corners with LiO_4 tetrahedra and form the 3D-framework of the spinel structure (Amin et al., 2020; Bhatia et al., 2021). $LiNi_{0.5}Mn_{1.5}O_4$ exists in two crystallographically different polymorphs, that is the face-centered cubic phase with space group $Fd\overline{3}m$ and the primitive cubic phase with space group $P4_332$. Depending on the synthesis conditions one or the other is formed. Ni and Mn can either be ordered in respectively the 4a and 12d sites of an ordered $P4_332$ space group or be randomly distributed in the 16d sites of a disordered $Fd\overline{3}m$-type unit cell (Amin & Belharouk, 2017; Bhatia et al., 2021). Both can be seen in Figure 2.7.

The ordered structure can be obtained by performing a synthesis process under oxygen or by post-annealing in air below 700 °C. The disordered structure is formed by preparation routes employing a higher synthesis temperature (over 700 °C).

This "high temperature polymorph" always goes together with the presence of a rock impurity phase. The impurity phase has been attributed to either Ni_xO, $Li_xNi_{1-x}O$ or $(LiNiMn)_xO$ and

[4] A rock salt structure is an ionic crystal structure in which cations have a face-centred cubic arrangement and anions occupy the octahedral holes ("Rock salt structure", n.d.).

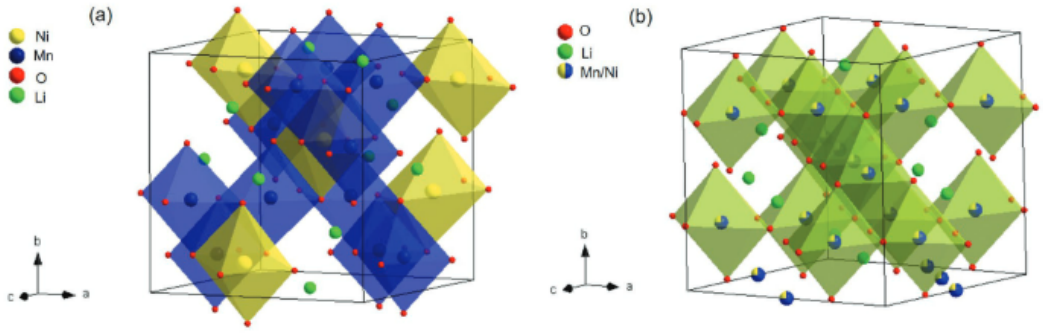

Figure 2.7: The crystal structure of a) ordered and b) disordered LNMO (Sun et al., 2022).

simultaneously shows an oxygen deficiency within the spinel. So with this in mind, the disordered structure has a different stoichiometry than the ordered structure (oxygen vacancies and nickel content lower than 0.5) and is often represented by $LiNi_{0.5}Mn_{1.5}O_{4-\delta}$ instead of $LiNi_{0.5}Mn_{1.5}O_4$ (Wang et al., 2011).

Next to that, the high calcination temperature needed to obtain the disordered structure sometimes leads to the reduction of the Mn oxidation state from +4 to +3. In the ideal case, the oxidation state of Mn in LNMO is fixed at +4, resulting in only the Ni^{2+}/Ni^{4+} redox couple during the charge/discharge process. Mn^{3+} participates in the redox, which results in a plateau at around 4 V on charge and discharge. The ordered structure on the other hand only contains Mn^{4+}, leading to the perfect $LiNi^{2+}{}_{0.5}Mn^{4+}{}_{1.5}O_4$ crystal structure. This is because of the annealing process making the oxidation state of Mn change from +3 to +4. So, the ordered structure exhibits a flat voltage profile at around 4.7 V and no plateau at the 4 V region (Kim et al., 2004).

As a result of $LiNi_{0.5}Mn_{1.5}O_{4-\delta}$ showing the Mn^{3+}/Mn^{4+} redox couple, it was initially believed that it would have relatively poor electrochemical performances compared to $LiNi_{0.5}Mn_{1.5}O_4$ because of the presence of Jahn-Teller ions (Mn^{3+}). However, despite these ions, the disordered material shows superior electrochemical performances. The Li/ $LiNi_{0.5}Mn_{1.5}O_{4-\delta}$ cell exhibits a higher discharge capacity than the Li/$LiNi_{0.5}Mn_{1.5}O_4$ cell at high rates (Kim et al., 2004).

2.5 Chemical diffusion coefficient

To optimize lithium-ion batteries it is crucial to study the kinetic parameters which control the rate performance of the Li intercalation electrodes. Lithium diffusion in the electrodes plays a vital role that determines the rate at which a battery can be charged and discharged (Xia et al., 2009). During an electrochemical reaction a lithium intercalation process takes place. This process involves multiple steps (Nikitina, 2020; Soult, 2023):

- Mass transport

  Mass transport includes the diffusion of Li^+ ions through the electrolyte and the solid electrode.

- Ion (de)solvation

  Ions are (de)solvated from the electrolyte in the vicinity of the electrode/electrolyte interface.

- Ion adsorption or desorption

  Ions are adsorbed or desorbed at the electrode surface (with adsorption this forms adions)

- Charge transfer

  Charge transfer involves two processes. On the one hand the transfer of an electron from the current collector to the redox active metal center in an intercalation host. On te other hand the transfer of a metal ion from the bulk of the solution into the intercalation compound.

These steps are illustrated in Figure 2.8 for Li^+ intercalation during charge and discharge at the positive electrode.

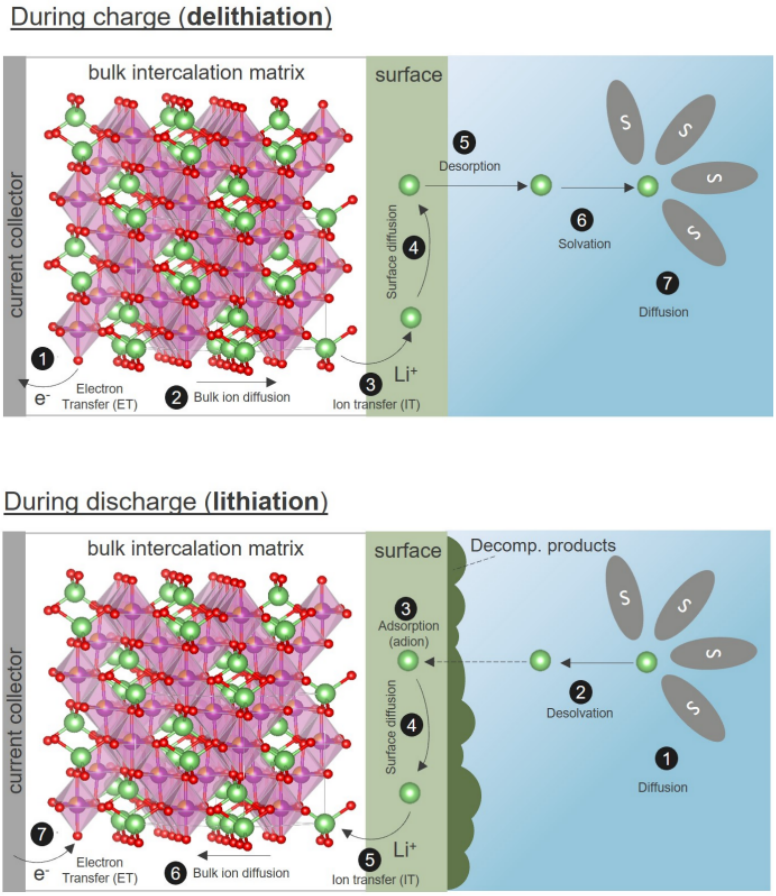

Figure 2.8: The schematic representation of the different steps in the electrochemical process of intercalation of Li^+ in a battery electrode (Soult, 2023).

Each of these steps happens at a certain rate that depends on factors inherent to the system and the experimental conditions. The slowest step will be the rate-limiting step and defines the overall rate of the reaction. Mass transfer will often be this rate-limiting step and can occur through diffusion, migration or convection. Diffusion will naturally take place in a medium when

there is a gradient in chemical potential caused by a gradient in concentration of a certain species. This is described by Fick's first law (Soult, 2023):

$$J_d = -\tilde{D}\frac{\delta c_i(x)}{\delta x} \tag{2.1}$$

With:

- J_d = the diffusion flux of species i
- $\tilde{D}$ = the chemical diffusion coefficient of species i
- c_i = the concentration of species i
- x = the position in the electrode (with x=0 at the electrode/electrolyte interface)

The chemical diffusion coefficient is used when the chemical composition varies in the diffusion zone over a certain range. This means the diffusing atoms will experience different chemical environments and thus have different diffusion coefficients. This situation is called interdiffusion or chemical diffusion. The symbol $\tilde{D}$ is used to indicate that the diffusion coefficient is concentration-dependent and is called the chemical diffusion coefficient. In this work it will also be referred to as the diffusion coefficient (Mehrer, 2007).

Fick's second law predicts how diffusion will change the concentration with respect to time and is given by:

$$\frac{\delta c_i(x,t)}{\delta t} = \tilde{D}\frac{\delta^2 c_i(x,t)}{\delta x^2} \tag{2.2}$$

LNMO has a spinel structure, which means the diffusion path will be different than for $LiCoO_2$ which has a layered structure. In spinel LNMO ($Fd\bar{3}m$) Li diffuses by moving from an 8(a) site to the neighbouring empty octahedral 16(c) site, and then to the next 8(a) site. These 8a - 16c - 8a diffusion paths are three-dimensionally interconnected. A schematic representation is given in Figure 2.9.

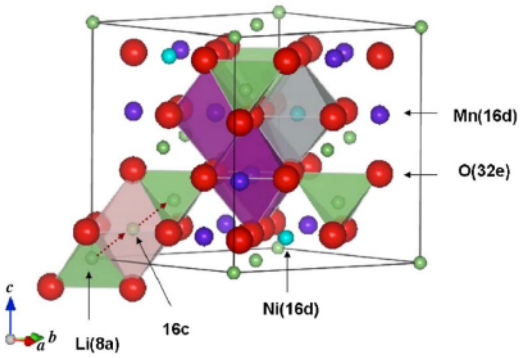

Figure 2.9: The schematic representation of the diffusion path of lithium in the spinel LNMO (Xia, Meng, et al., 2007).

The lithium diffusion coefficient can be determined using different techniques. The ones used in this work are: the Galvanostatic Intermittent Titration Technique (GITT), the Potentiostatic Intermittent Titration Technique (PITT) and the Intermittent Current Interruption (ICI).

Chapter 3

Objectives

When studying literature one finds a large variation in order of magnitudes for the lithium diffusion coefficient in LNMO. Reliable and quantitative values are lacking. This forms a problem when trying to model the optimal design for a battery containing LNMO as positive electrode. Modelling needs a good, quantitative description of the lithium diffusion coefficient. So, the objective of this thesis is to obtain a reliable result for the lithium diffusivity in LNMO.

Therefore, thin film LNMO electrodes are used. The thin film electrodes are composed of the pure material, such that the influence of other components like conductive additives or binders can be avoided. Furthermore, thin film electrodes allow to have a good estimation of the contact area between the electrolyte and active material, which can be approximated by the thin film surface (Shi et al., 2010; Xia et al., 2009).

This thesis will determine the lithium diffusion coefficient using three different techniques: the Galvanostatic Intermittent Titration Technique (GITT), the Potentiostatic Intermittent Titration Technique (PITT) and Intermittent Current Interruption (ICI). By using thin film electrodes instead of composite electrodes, it is expected that the difference in value between the diffusivities obtained with the different techniques will be smaller compared to what is the case in literature at the moment.

Furthermore, this thesis will describe the evolution of the diffusion coefficient as a function of potential.

Next to that, this work will try to establish the most reliable method out of the three to determine the diffusion coefficient in thin film electrodes.

Finally, the influence of the thin film electrode thickness on the electrochemical behaviour will also be explored.

Chapter 4

Methods to determine the diffusion coefficient

4.1 Galvanostatic Intermittent Titration Technique (GITT)

The Galvanostatic Intermittent Titration Technique is developed by Weppner and Huggins and is a well adopted method to determine the lithium diffusion coefficient that combines transient perturbation and steady-state measurements (Rahim et al., 2022).

The chemical diffusion coefficient of species A can be investigated in a mixed conductor $A_{y+\delta}B$ (δ symbolizes the deviation from the ideal stoichiometric composition) by the use of a galvanic cell with $A_{y+\delta}B$ as one electrode, as shown in Figure 4.1. In this figure, A and A° represent respectively the counter and reference electrodes. Instead of pure A, another material with a different activity than A may also be used for these electrodes (Weppner & Huggins, 1977).

An electric current I is driven through the galvanic cell by an external source. This current determines the transport of the relevant mobile ionic species within the sample just inside the phase boundary with the electrolyte (where x = 0, see Figure 4.1) (Weppner & Huggins, 1977).

The current[1] is given by:

$$I = -Sz_i q\tilde{D}\frac{\delta c_i}{\delta x}|_{x=0} \tag{4.1}$$

With:

- S = the area of sample-electrolyte interface
- z_i = the charge number (valence) of species i
- q = the elementary charge

In this equation i is A or B depending on which one has the predominant conductivity.

The principles underlying the GITT method for the determination of the diffusion coefficient of a mixed conductor are shown in Figure 4.2. The method starts with a sample of known stoichiometric composition and with the galvanic cell in thermodynamic equilibrium. This means the concentrations of all species are homogeneous in the electrode $A_{y+\delta}B$, corresponding to cell voltage E_0. A constant current I_0 is then applied to the cell at a time t_0 during a time τ. Following equation 4.1, this constant current produces a constant concentration gradient $\frac{\delta c_i}{\delta x}$ within the

[1] Equation 4.1 is based on Fick's first law (J = -$\tilde{D}$ dc/dx)

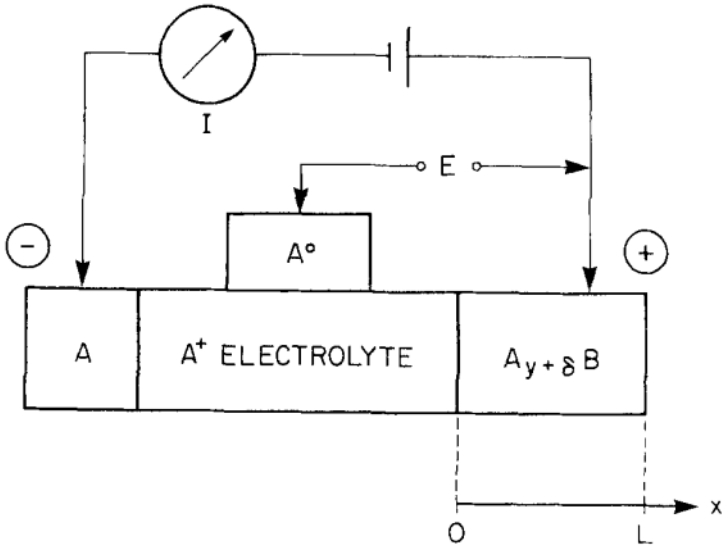

Figure 4.1: The schematic illustration of an experimental galvanic cell arrangement. The electrolyte-sample interface is at x = 0. The sample thickness is L (Weppner & Huggins, 1977).

$A_{y+\delta}B$ at the phase boundary with the electrolyte (x = 0). To be able to maintain this constant concentration gradient, the applied cell voltage increases (or, depending on the direction of the current, decreases) with time. However, due to the current flux through the electrolyte and the interface, a voltage step corresponding to the IR drop is superimposed. The magnitude of this step does only depend on the position of the electrode and remains constant with time. After a time τ the current flux is interrupted. The composition within $A_{y+\delta}B$ becomes homogeneous again by diffusion of the mobile species. However, the cell voltage goes to a new steady-state value E_1. Due to a change in stoichiometry $\Delta\delta$ caused by the coulometric titration of A ions in the sample by the current, A has a new activity in the sample which influences the cell voltage (Weppner & Huggins, 1977).

$\Delta\delta$ is given by:

$$\Delta\delta = \frac{I_0 \tau M_B}{z_A m_B F}|_{x=0} \tag{4.2}$$

With:

- M_B = the atomic weight of B
- m_B = the mass of component B in the sample
- I_0 = the constant current
- F = Faraday's constant (96 485 C/mol)

After the electrode reaches equilibrium again, the procedure can be repeated, but starting from a new cell voltage E_1. This process may be continued until a phase change occurs in the electrode or the electrolyte decomposes or becomes electronically conductive.

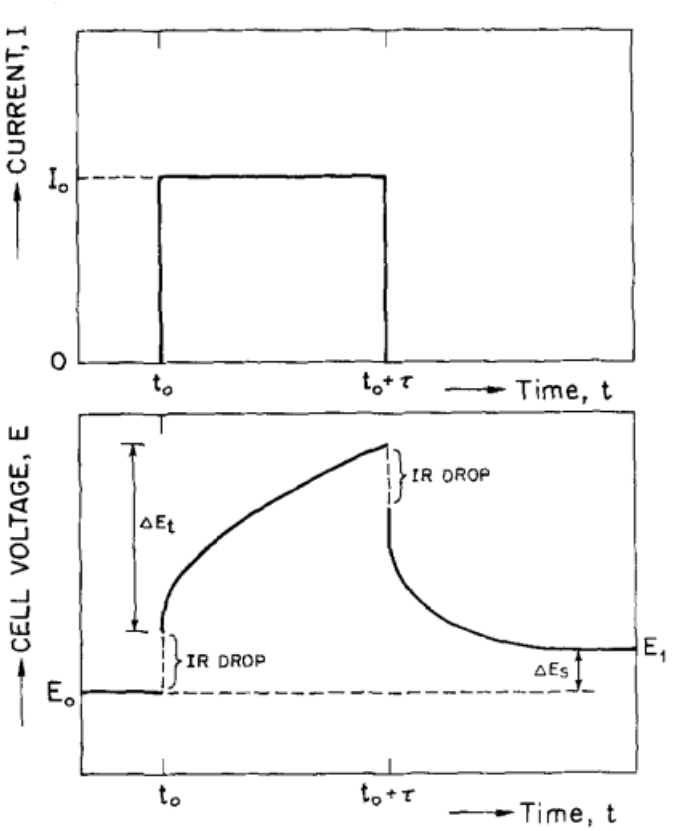

Figure 4.2: The schematic illustration of a single step of the galvanostatic intermittent titration technique (GITT). ΔE_t is the total transient voltage change of the galvanic cell for a certain applied galvanostatic current I_0 during a time τ. ΔE_s is the change of the steady-state voltage of the cell for this step (Weppner & Huggins, 1977).

To calculate the cell voltage E[2] as a function of time t during which the current is applied, the time dependence of the concentration c_i at the interface (x=0) needs to be determined. This can be done by solving Fick's second law (Weppner & Huggins, 1977):

$$\frac{\delta c_i(x,t)}{\delta t} = \tilde{D}\frac{\delta^2 c_i(x,t)}{\delta x^2} \tag{4.3}$$

With the initial and boundary conditions:

$$c_i(x, t=0) = c_0 \qquad (0 \leq x \leq L) \tag{4.4}$$

$$-\tilde{D}\frac{\delta c_i}{\delta t}|_{x=0} = \frac{I_0}{S z_i q} \qquad (t \geq 0) \tag{4.5}$$

$$\frac{\delta c_i}{\delta t}|_{x=L} = 0 \qquad (t \geq 0) \tag{4.6}$$

[2]The cell voltage can be determined using the Nernst equation which is dependent on the thermodynamic activity of neutral A in the $A_{y+\delta}B$ sample at the interface with the electrolyte. The activity is in its turn dependent on the concentration.

Condition 4.5 is deduced from Equation 4.1. The last condition is due to the fact that the right-hand phase boundary of the sample is assumed to be impermeable. By solving differential equation 4.3 with conditions 4.4 - 4.6 eventually an expression for the diffusion coefficient can be found (Weppner & Huggins, 1977):

$$\tilde{D} = \frac{4}{\pi}\left(\frac{V_M}{SFz_i}\right)^2 \left(I_0\left(\frac{dE}{d\delta}\right) / \left(\frac{dE}{d\sqrt{t}}\right)\right)^2 \qquad t << L^2/\tilde{D} \tag{4.7}$$

If the change in steady-state voltage (E_1 - E_0 = ΔE_S) over a single galvanostatic titration is small (by using a sufficiently small current), $dE/d\delta$ may be considered to be constant. Therefore, it may be replaced by the ratio of the finite quantities, $\Delta E_S/\Delta\delta$. Then Equation 4.2 can be inserted into Equation 4.7, which gives (Weppner & Huggins, 1977):

$$\tilde{D} = \frac{4}{\pi}\left(\frac{m_B V_M}{M_B S}\right)^2 \left(\frac{\Delta E_S}{\tau\left(\frac{dE}{d\sqrt{t}}\right)}\right)^2 \qquad t << L^2/\tilde{D} \tag{4.8}$$

If E vs.$\sqrt{t}$ shows the expected straight line behaviour over the entire time period of the current flux, Equation 4.8 can be further simplified (Weppner & Huggins, 1977):

$$\tilde{D} = \frac{4}{\pi\tau}\left(\frac{m_B V_M}{M_B S}\right)^2 \left(\frac{\Delta E_S}{\Delta E_t}\right)^2 \qquad t << L^2/\tilde{D} \tag{4.9}$$

Where ΔE_t is the total change in cell voltage E during the current pulse without the IR drop (Weppner & Huggins, 1977).

4.2 Potentiostatic Intermittent Titration Technique (PITT)

In the PITT method a sudden step in the potential across the cell is imposed, as can be seen in Figure 4.3. For this technique the same cell as represented in Figure 4.1 can be used. It is assumed that the concentration of mobile species A is initially uniform over the electrode, which corresponds to an equilibrium voltage E_0 with respect to a reference electrode. By applying a voltage step, ΔE, at t= 0 between the sample $A_{y+\delta}B$ and the reference electrode, a new activity of A is imposed on the electrode surface (of $A_{y+\delta}B$). Now, there is a new concentration of A in $A_{y+\delta}B$ at the electrode-electrolyte interface (x=0) represented by C_S. Due to the concentration gradient that goes along with this, chemical diffusion occurs within $A_{y+\delta}B$. To keep the surface concentration constant at the imosed value C_S until the electrode reaches this concentration everywhere, electroactive species must be continuously supplied by transport through the electrolyte. The magnitude of this transient current I gives a measure for the chemical diffusion flux as a function of time. For one-dimensional transport, as for GITT, one can start from Fick's second law to describe the chemical diffusion process (Wen et al., 1979):

$$\frac{\delta c_A(x,t)}{\delta t} = \tilde{D}\frac{\delta^2 c_A(x,t)}{\delta x^2} \tag{4.10}$$

The initial and boundary conditions are:

$$c_A(x, t=0) = c_0 \qquad (0 \le x \le L) \tag{4.11}$$

$$C_A = C_S \qquad (x=0), (t>0) \tag{4.12}$$

$$\frac{\delta c_A}{\delta t}|_{x=L} = 0 \qquad (t \ge 0) \tag{4.13}$$

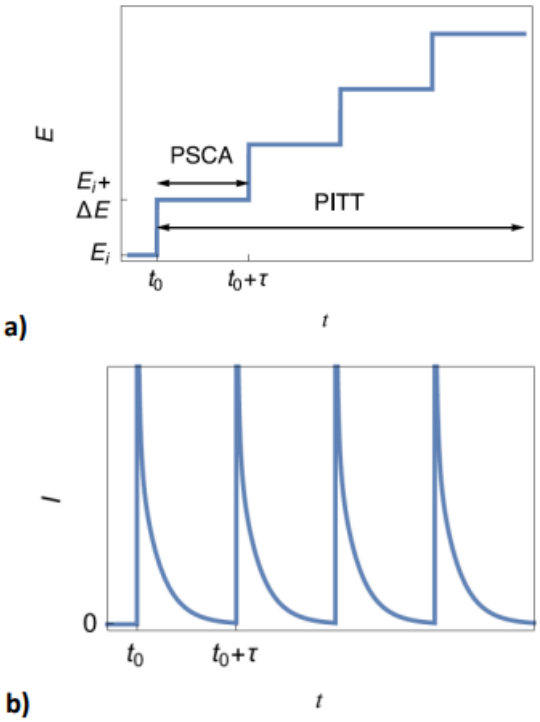

Figure 4.3: a) Principle of the PITT, with PSCA a potential step of constant height b) The typical current response (Murer et al., 2021).

A combination of the expression for the electric current dependent on time (given in Equation 4.1) and the solution of the differential equation 4.10 using conditions 4.11 - 4.13, gives two possible expressions for the current. On the one hand the short-time or Cottrell relationship (Montella, 2002; Wen et al., 1979):

$$I(t) = -FS(C_S - C_0)\frac{\sqrt{\tilde{D}}}{\sqrt{\pi t}} \qquad t << L^2/\tilde{D} \tag{4.14}$$

On the other hand there is the exponential decay at long times:

$$I(t) = -2FS(C_S - C_0)\frac{\tilde{D}}{L}exp(-\frac{\pi^2\tilde{D}t}{4L^2}) \qquad t >> L^2/\tilde{D} \tag{4.15}$$

Therefore, in the initial stage of diffusion (Equation 4.14) the chemical diffusion coefficient can be determined from the slope of the linear plot of I vs. $1/\sqrt{t}$ (for short times), provided that the concentration difference is known, or the change in charge for each step can be determined.

$$\tilde{D} = \pi\left(\frac{Sl_{I,st}}{FS\Delta c}\right)^2 = \pi\left(\frac{Sl_{I,st}L}{\Delta Q}\right)^2 \qquad (t << L^2/\tilde{D}) \tag{4.16}$$

In the long time approximation, the chemical diffusion coefficient can be determined from either the slope of a linear plot of ln(I) vs. t without needing knowledge of the concentration difference, or from the intercept on the ln(I) axis at t=0 on the same plot if C_S - C_0 is known

(Wen et al., 1979). The expression used the most for the PITT technique is the following (Xie et al., 2009; Zhu & Wang, 2010):

$$\tilde{D} = -\frac{dln(I(t))}{dt}\frac{4L^2}{\pi^2} \qquad (t >> L^2/\tilde{D}) \tag{4.17}$$

A disadvantage of this technique is that the ohmic voltage drop in the bulk electrolyte varies with time and cannot be readily eliminated from the voltage difference that is imposed (Wen et al., 1979).

4.3 Intermittent Current Interruption (ICI)

For GITT an equilibrium condition is required before applying the next current pulse. In order to reach this equilibrium condition the cell needs to be relaxed substantially longer than the time spent on the current pulse. This makes GITT a very time consuming technique. However, recently the Intermittent Current Interruption (ICI) technique has been proposed as a faster alternative to GITT. This method introduces repeating transient current interruptions while the cell is under a constant current. The voltage response during these current interruptions is monitored, which also follows a linear relationship with the square root of time. Through this linear regression, quantities describing the time-independent and time-dependent parts of the resistance can be derived, which are termed internal resistance and diffusion resistance coefficient respectively. It has been shown that the diffusion resistance coefficient is proportional to the coefficient of the Warburg element, which is used when fitting electrochemical impedance spectrocopy measurements (EIS). This Warburg element describes both the capacitive behaviour in porous electrodes and diffusion processes, so it is a logical consequence that the ICI method can characterize diffusion processes in an electrochemical system as well. Since the ICI method does not require the cell to be in an equilibrium state, the most time consuming part of the GITT method (namely the relaxation period) can be omitted (Chien et al., 2021, 2023; Geng et al., 2022).

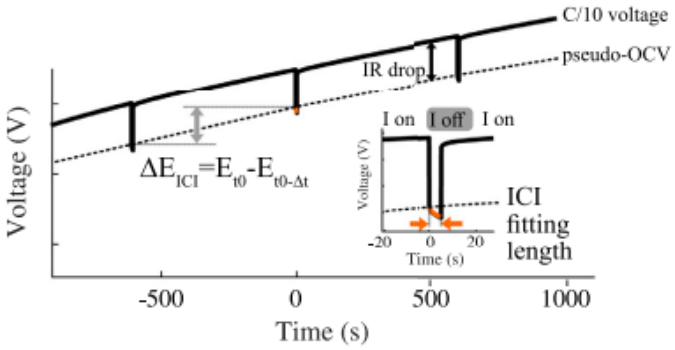

Figure 4.4: The voltage response during interruption of the current. t_0 is the time when the current is interrupted in the region of interest, and Δt is the time interval between two current interruptions(Geng et al., 2022).

The ICI method was originally designed for continuous resistance measurements. The change in potential after the current has been switched off ($\Delta t = 0$) can be expressed as following (Chien et al., 2023):

$$\Delta E(\Delta t) = E(\Delta t) - E_I = -IR - Ik\sqrt{\Delta t} \tag{4.18}$$

With:

- E_I = the potential right before the current is switched off
- R = the internal resistance
- k = the diffusion resistance

R and k can be acquired through the linear regression of ΔE against $\sqrt{\Delta t}$. The ICI method renders the diffusion coefficient using the same equation as the GITT method, only some parameters have a different meaning now:

$$\tilde{D} = \frac{4}{\pi}\left(\frac{m_B V_M}{M_B S}\right)^2 \left(\frac{\Delta E_{ICI}}{\Delta t\left(\frac{dE}{d\sqrt{t}}\right)}\right)^2 \tag{4.19}$$

Now, $dE/d\sqrt{t}$ is fitted during the zero current period and $\Delta E_{ICI}/\ \Delta t$ is estimated from a pseudo open circuit potential, which is shown in Figure 4.4 (Geng et al., 2022).

Chapter 5

Materials and methods

5.1 Materials

5.1.1 Thin film electrode

In this study a thin film electrode is used. This thin film is deposited using the radio frequency (RF) sputtering technique. The active material is configured in a thin layer of around 70 nm. Depending on the sputtering time, the thickness of the active material will be different. When sputtering for 2 hours the thickness of 70 nm is achieved, which is confirmed by Figure 5.1 (Soult, 2023).

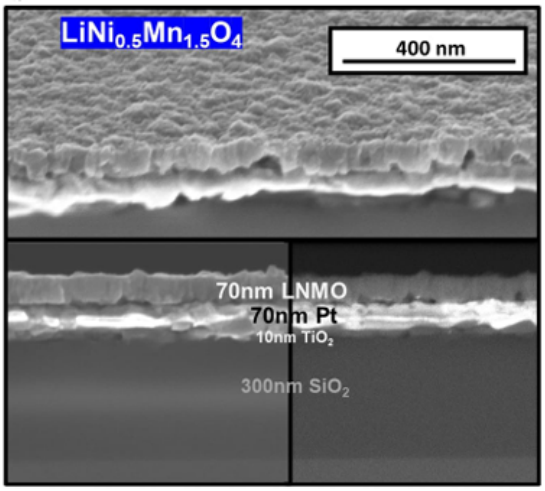

Figure 5.1: The tilt and cross-section SEM image of LNMO on Pt / TiO_2 / SiO_2 / Si substrate. This confirmes the LNMO layer having a thickness of around 70 nm (Soult, 2023).

5.1.2 Electrochemical setup

All the electrochemical experiments using thin films in this thesis were done using the same setup. This configuration exists out of a custom-made polytetrafluorethylene (PTFE) or Teflon

cell designed and manufactured by imec, compromising three electrodes and two cavities. One of the cavities is the counter electrode compartment (CE), while the other one holds the reference electrode (RE). The thin film is the working electrode and is positioned at the bottom of the Teflon cell. The cavities are interconnected with a channel, allowing ion exchange between the compartments during the cell operation. The cavities are filled with liquid electrolyte and leakage is prevented by an O-ring that seals the joint between the Teflon cell and the thin film. This setup can be seen in Figure 5.2.

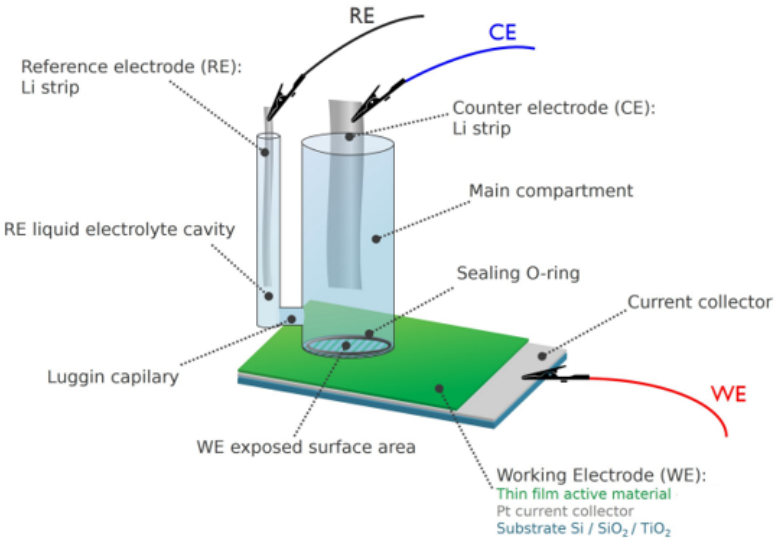

Figure 5.2: The three-electrode cell used for all the electrochemical experiments including thin film electrodes (Soult, 2023).

Both the counter and reference electrode are lithium strips. So, the potential is always measured vs. Li^+/Li. The electrolyte used is 1M $LiPF_6$ in propylene carbonate (PC). The area of the working electrode exposed to electrolyte is 0.785 cm^2.

5.2 Methods

The different techniques are executed in an argon-filled glovebox (Jacomex GP[Concept]) with a potentiostat. This potentiostat is the SP-200 model from Bio-Logic SAS. The calculations to determine the diffusion coefficient from the data are done using Jupyter Notebook (Anaconda 3) in the programming language Python, using libraries numpy, matplotlib, pandas and scipy. The data is also analysed using EC-Lab.

The general scheme of an experiment is given in Figure 5.3. Because every experiment is started by measuring the open circuit potential and doing two cyclic voltammetry cycles, the GITT, PITT and ICI experiments do not start at a time equal to zero.

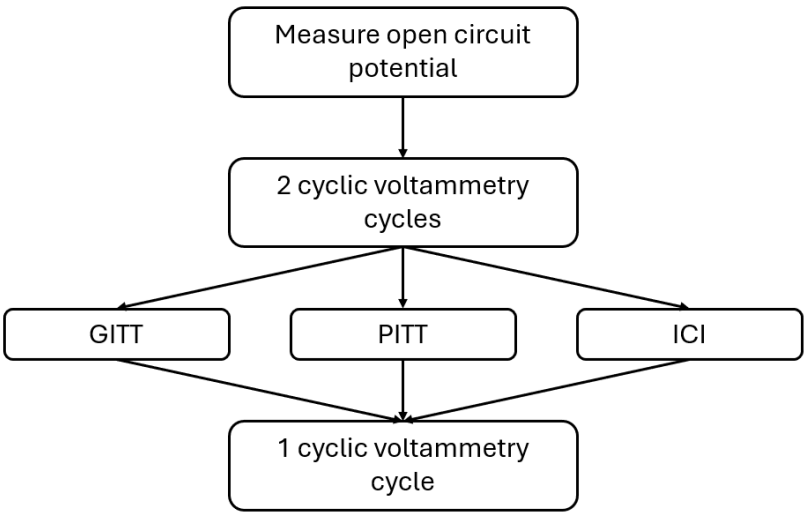

Figure 5.3: The general scheme of an experiment.

5.2.1 Cyclic voltammetry

With cyclic voltammetry the current is recorded by linearly going over a range of potentials from lower to higher and from higher to lower value. Here, two cycles are executed at a rate of 1 mV/s. The first cycle starts at the open circuit potential, goes to a maximum of $E_1 = 4.85$ V and then goes back until $E_2 = 3.8$ V. For the second cycle the same E_1 and E_2 are used.

5.2.2 GITT

With the Galvanostatic Intermittent Titration Technique pulses of current are applied and the change in potential is measured. Different values for the parameters were tried to find the optimum ones. The main ones are given in Table 5.1.

Table 5.1: The settings used in the different experiments for the GITT technique.

Experiment	**I_0 [µA]**	**Pulse time [min]**	**Relaxation time [min]**	**Cycles**
1	2.5	3	15	40
2	3	3	30	40
3	5	3	45	40

5.2.3 PITT

With the potentiostatic intermittent titration technique steps in potential are applied and the change in current is measured. To find the optimum settings, different parameters were varied. The main experiments can be found in Table 5.2.

Table 5.2: The settings used in the different experiments for the PITT technique.

Experiment	**Thickness [nm]**	**ΔE [mV]**	**Pulse time [min]**	**Cycles**
1	70	10	4	60
2	70	10	9	60
3	70	10	4	120

5.2.4 ICI

The intermittent current interruption technique is deviated from the GITT technique. Here, a constant current is applied with interruptions of a few seconds for each sequence. Again, different values for some parameters were tested to find the optimum ones. The main experiments can be found in Table 5.3.

Table 5.3: The settings used in the different experiments for the ICI technique.

Experiment	**Thickness [nm]**	**I_0 [μA]**	**Pulse time [min]**	**Relaxation time [s]**	**Cycles**
1	70	0.7	5	10	30
2	70	1	5	10	30
3	70	1.5	5	10	60
4	210	1.5	5	10	60
5	280	1.5	5	10	60

Chapter 6

Results and discussion

6.1 Cyclic Voltammetry

The result of the cyclic voltammetry test is given in Figure 6.1. By going to a higher voltage, the battery is charged which means the positive electrode is delithiated. So, the peaks with a positive current represent oxidation reactions, while the peaks with a negative current represent reduction reactions.

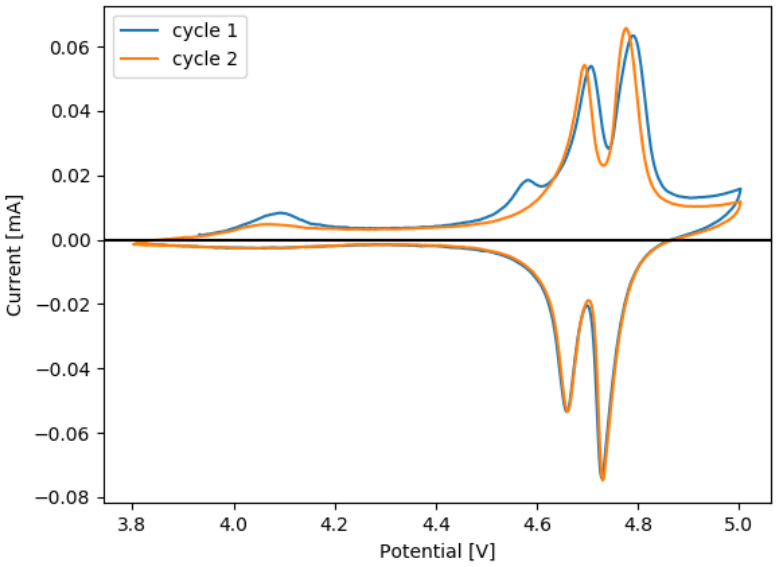

Figure 6.1: Cyclic voltammogram of the thin film LNMO electrode, where 2 cycles are completed. The two maxima are taking place at potentials of 4.69 and 4.77 V and the two minima at 4.66 and 4.73 V.

In Figure 6.1 two cycles of charging and discharging are depicted. One can see that the first cycle shows some additional peaks in comparison to the second cycle. These additional peaks are

only present in the charging part (positive current) of the first cycle and not in the discharging part (negative current). These peaks represent non-reversible reactions that only take place during charging in the first cycle. The reactions that are always taking place during charge and discharge are depicted in the second cycle, given in Figure 6.2. Three peaks are present for both the charging and discharging part of the second cycle. They are indicated by red circles. The three oxidation peaks have potentials of respectively 4 V, 4.69 V and 4.77 V. The three reduction peaks are taking place at potentials of respectively 4 V, 4.66 V and 4.73 V. These peaks can be explained based on the reactions taking place. The oxidation peaks at 4.69 V and 4.77 V are caused by respectively the Ni^{2+}/Ni^{3+} and the Ni^{3+}/Ni^{4+} redox couple. The small peak at around 4 V can be attributed to the Mn^{3+}/Mn^{4+} redox couple, caused by the small amount of Mn^{3+} present in disordered LNMO (W. Liu et al., 2017). With this cyclic voltammetry test, one can examine if the material works correctly. Based on literature, one expects to obtain three oxidation and reduction peaks at the potentials represented in Figure 6.2. If this is not the case, this is an indication that something is wrong with the electrode. Besides that, doing a cyclic voltammetry test is necessary to already have the non-reversible reactions from the first cycle, such that these do not influence the measurements of the diffusion coefficient.

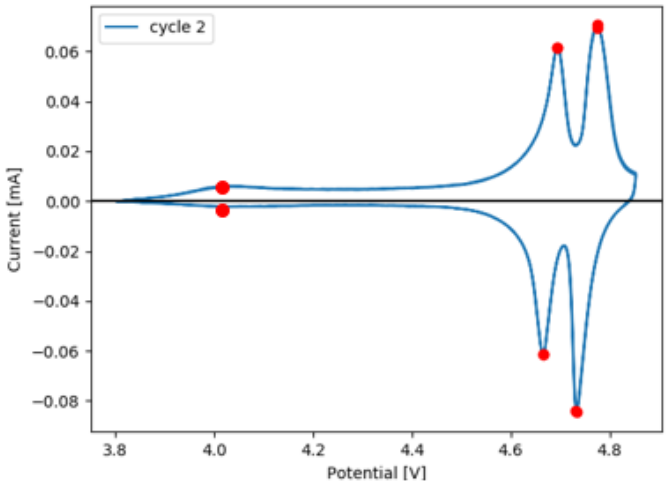

Figure 6.2: Cyclic voltammogram of the thin film LNMO electrode. Only the second cycle is shown here.

6.1.1 Comparison different electrode thicknesses

The influence of the thickness of the thin film LNMO electrode on the electrochemical behaviour is studied as well. In Figure 6.3 the second cycle of the cyclic voltammogram is given for electrode thicknesses of 70, 140, 210 and 280 nm.

When looking at Figure 6.3, one can see that with increasing thickness the peak height increases as well. Furthermore, the ratio of both the oxidation and reduction peaks in the high-voltage window changes starting from a thickness of 210 nm. Figure 6.4 is a zoom in on the peak taking place around 4 V. One can notice a shift in potential starting from an electrode thickness of 210 nm for this peak. Next to that, the data for an electrode thickness of 280 nm is noisier than for the other thicknesses.

As there is an increase in capacity with increasing thickness, it is expected that the peak

height increases as well. Furthermore, the oxidation peak corresponding to the Mn^{3+}/Mn^{4+} redox couple moves towards a higher potential with increasing thickness. This means that with increasing thickness, the oxidation of Mn^{3+} to Mn^{4+} takes place at a higher potential. Next to that, the behaviour during the nickel redox couples changes as well with increasing thickness. Starting from a thickness of 210 nm the peak corresponding to the Ni^{2+}/Ni^{3+} redox couple becomes larger than the one corresponding to Ni^{3+}/Ni^{4+}. From this, one can deduce that starting from a certain thickness more Ni^{2+} oxidizes to Ni^{3+} than Ni^{3+} to Ni^{4+}. This is observed for both the oxidation and reduction peaks. Thus, around a thickness of 200 nm there is a change in behaviour in the thin film LNMO electrodes.

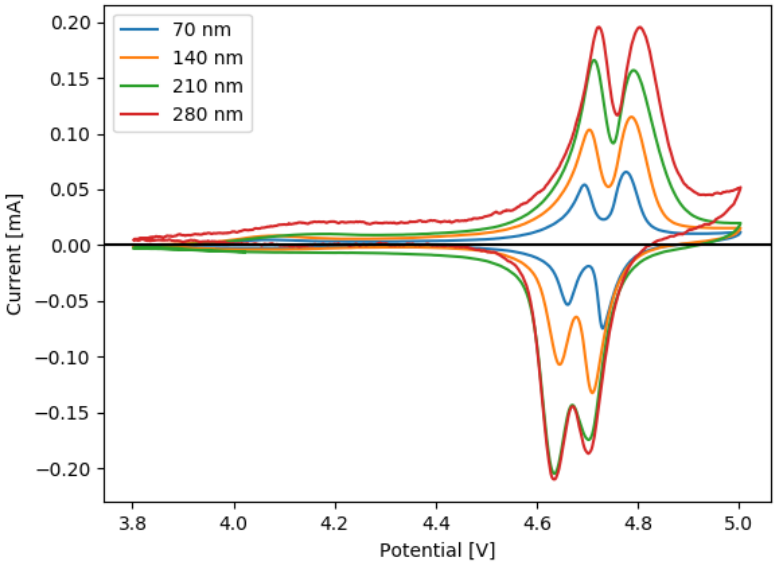

Figure 6.3: Cyclic voltammogram of the thin film LNMO electrode for different thicknesses. The second cycle is given here.

6.2 GITT

For the Galvanostatic Intermittent Titration Technique current pulses are applied and the potential response is measured. This technique uses Equation 4.9 to calculate the lithium diffusion coefficient. In order to justify the use of Equation 4.9, some assumptions made, need to be examined. First of all, prior to each pulse the material composition should be homogenized. Therefore, the battery should be charged in a lot of steps to ensure a small change in stoichiometry of the positive electrode. Furthermore, the relaxation time should be larger than the pulse time, making sure the lithium concentration goes to an equilibrium again. Secondly, changes of molar volume with composition should be negligible. Intercalation compounds such as LNMO typically undergo low volume changes in the range of 3 to 6 % during Li^+ (de)intercalation. This means that for thin films with a thickness of 70 nm the absolute volume changes are minimal (less than 5 nm) (Soult et al., 2022). Thirdly, the reaction must be limited by solid-diffusion

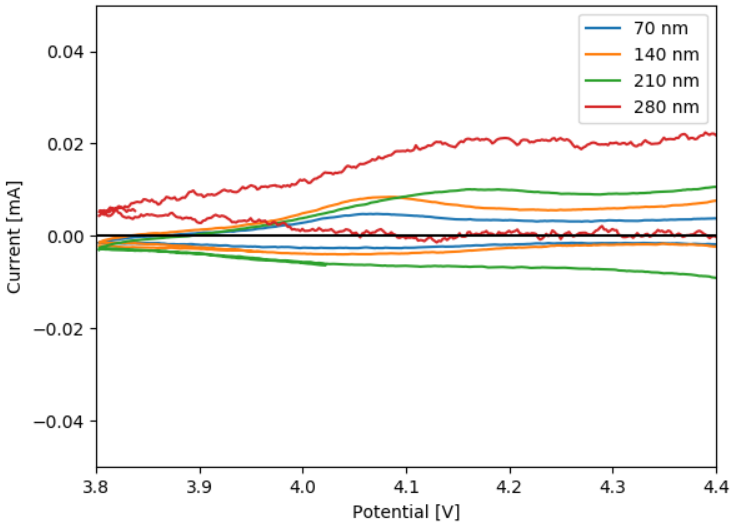

Figure 6.4: A zoom in on the peak taking place around 4 V of the second cycle of the cyclic voltammogram.

(diffusion is the rate-limiting step). However, as solid diffusion is often the rate limiting step this requirement is rarely validated in reality. Finally, the method only complies for planar 1-dimensional semi-infinite systems. This is validated by making sure the pulse time is shorter than the time needed for diffusion through the electrode: $t << L^2/\tilde{D}$ (Kang & Chueh, 2021). However, this last assumption can only be validated when one has an idea of the value for the lithium diffusion coefficient in the thin film LNMO electrodes.

To optimize the measurement of the diffusion coefficient using GITT, iterative experimentation using different parameters was necessary. A first estimation of the optimum values for the parameters was done in the following way. The capacity of the LNMO samples is 1.37 µAh. When applying 40 pulses of 3 minutes the total charging time equals to 2 hours. To charge an LNMO sample in 2 hours a current of around 0.7 µA is needed. The 40 charging steps are necessary to ensure only small changes in stoichiometry for each step. Furthermore, a single pulse cannot be too long, otherwise the last assumption ($t << L^2/\tilde{D}$) will not be fulfilled. Therefore, a pulse time of 3 minutes is taken. Next to that, GITT needs a relaxation time that is long enough, such that the material composition is homogenized again prior to each pulse. So, in between the pulses of 3 minutes relaxation times of 15 minutes are implemented. However, with these settings the necessary potential of 4.8 V could not be reached. This can be explained based on that during the relaxation times the potential will decrease a small amount again towards an equilibrium. Taking this into account, the applied current must be larger to fully charge the battery. The best results were obtained for a current pulse of 3 µA applied for 3 minutes and a relaxation time of 30 minutes. For currents lower than 3 µA the potential of 4.8 V could not be reached. For currents higher than 3 µA, the potential response showed unusual behaviour.

Figure 6.5 shows the potential response to a current pulse for a current of 2.5 µA (with relaxation times of 15 minutes) and for a current of 3 µA (with relaxation times of 30 minutes). Each color represents a cycle existing out of a current pulse and relaxation. During the time the

current pulse is applied the potential rises to a higher value. After that, during the relaxation time, the potential decreases again and goes to an equilibrium. By observing the curve as a whole, one can see that the potential increases from around 3.8 V to 4.7 V or 4.8 V for respectively a current of 2.5 µA or 3 µA. With increasing potential, the rate at which the potential rises becomes smaller, until it finds an equilibrium. So, the potential goes to an equilibrium as a function of time around 4.7 V for a current pulse of 2.5 µA. This is not high enough to see the influence of the reactions taking place at 4.69 and 4.77 V. Therefore, the experiment was repeated with higher current pulses.

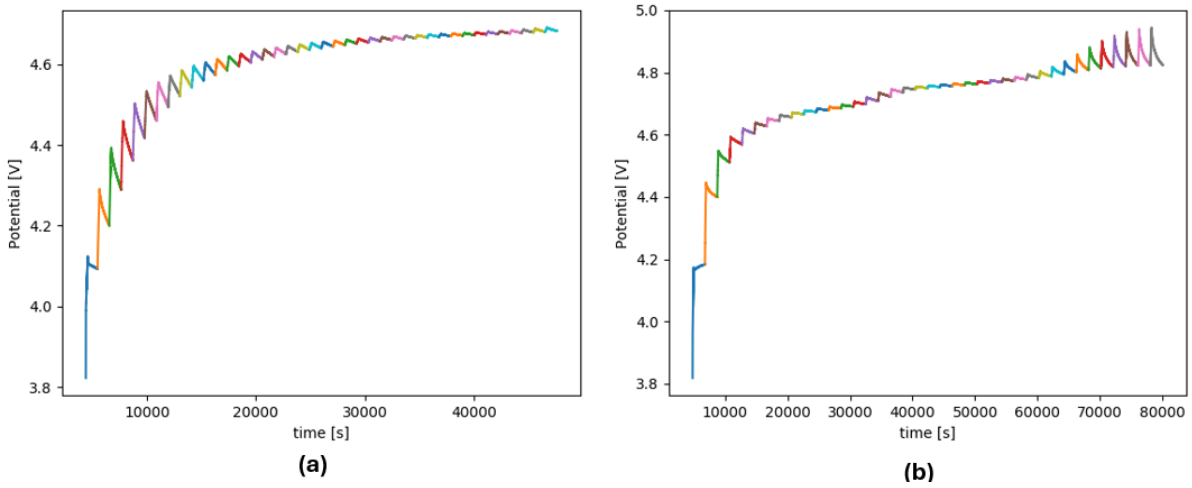

Figure 6.5: The potential response to a current step of (a) 2.5 µA and (b) 3 µA.

To determine the diffusion coefficient at different potentials from the curve where the potential is plotted as a function of time, the method described in section 4.1 can be used. This method uses Equation 4.9, wherefore ΔE_S and ΔE_t need to be determined for every step.

It is only justified to use Equation 4.9 (instead of Equation 4.8) when $\tau(dE/d\sqrt{t})$ can be replaced by ΔE_t. This is the case when linear behaviour is observed between the potential and $\sqrt{t}$ during the current pulse. Therefore, the potential is plotted as a function of the square root of time for the 20th cycle (out of 40 in total). This can be seen in Figure 6.6. This 20th cycle is a representation, the linear behaviour was validated for all cycles. With an R^2 value of 0.99 and 0.97 for a current pulse of 2.5 µA and 3 µA respectively, one can consider the behaviour to be linear.

In Figure 6.7 the evolution of the diffusion coefficient for both current pulses (2.5 µA and 3 µA) is depicted. In Figure 6.8 the averaged behaviour at a current pulse of 3 µA is represented with error bars. The diffusion coefficient shows a downward trend from 10^{-12} to 10^{-15} cm^2/s. Now, the last assumption ($t << L^2/\tilde{D}$) can be validated. As for the largest potential window the diffusion coefficient has an order of magnitude of 10^{-13} cm^2/s, this is taken as $\tilde{D}$. With a thickness of 70 nm, this results in a time that needs to be smaller than 490 seconds or 8 minutes, which means the last condition is valid.

From Figure 6.8 one can derive that at the beginning (potentials from 3.8 to 4.3 V) there is a slight decrease in diffusion coefficient, after which it increases a bit again until 4.5 V. This trend can be explained based on the activation barrier for Li ions to jump that first slightly increases and then decreases again. During diffusion Li migrates from its original tetrahedral 8a site to another one, through an intermediate empty octahedral 16c site. The total energy of the cell

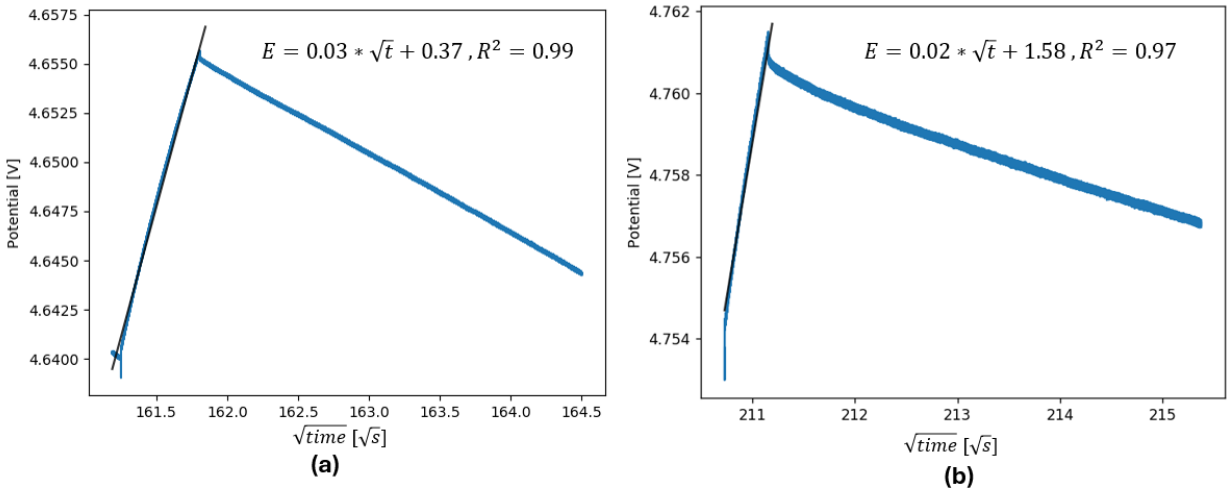

Figure 6.6: The potential vs. $\sqrt{t}$ for the 20th cycle shows a linear behaviour with a slope of (a) 0.03 and $R^2 = 0.99$ for a current pulse of 2.5 µA and (b) 0.02 and $R^2 = 0.97$ for a current pulse of 3 µA.

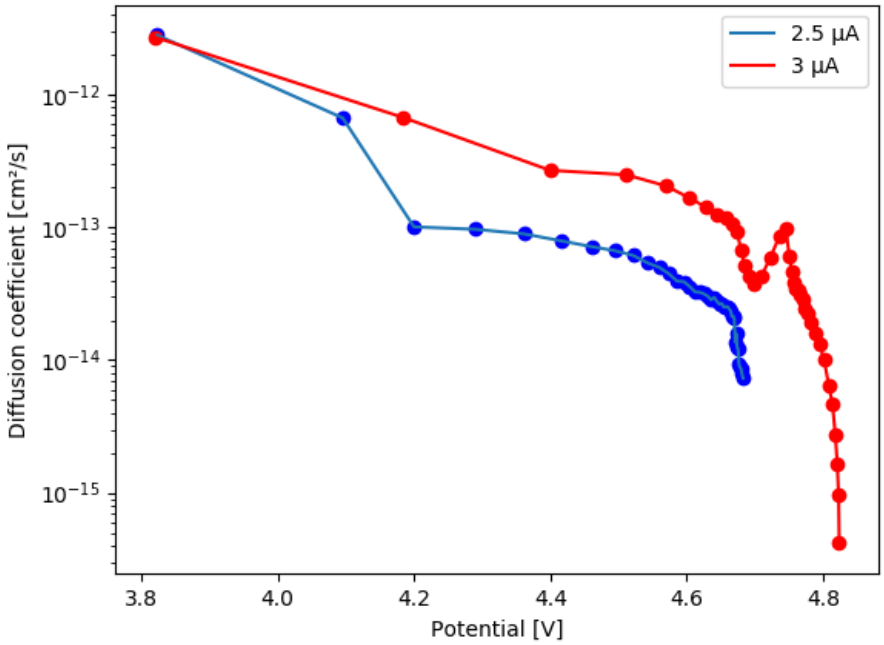

Figure 6.7: The evolution of the diffusion coefficient during charge (delithiation of the positive thin electrode) using the method which needs ΔE_S and ΔE_t for every step. It is plotted for a current pulse of 2.5 µA and 3 µA.

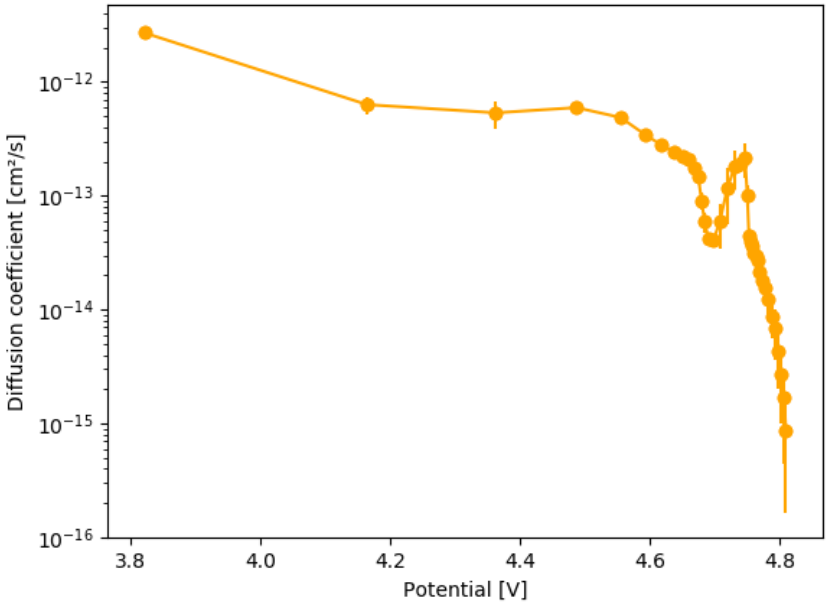

Figure 6.8: The evolution of the diffusion coefficient during charge (delithiation of the positive thin electrode) for a current pulse of 3 µA. This is the averaged behaviour over three experiments.

changes during this migration of the mobile lithium ion and reaches a maximum when Li ions are in the 16c sites. The energy difference between the initial state (8a) and the metastable state (16c) is considered as the Li diffusion activation barrier E_a (Bhattacharya & Van der Ven, 2010; Xu & Meng, 2010).

The variation in this activation barrier during charging (= delithiation) can have multiple causes. On the one hand the variation of the a-lattice parameter during delithiation. As lithium leaves the structure, more vacancies are created and Ni goes to a higher oxidation state which reduces the a-lattice parameter (or c-lattice parameter for layered structures). However, this influence is not as big for the spinel structure as for layered structures. In layered structures any drop of the c-lattice parameter reduces the distance between oxygen planes, resulting in an increase of the activation barrier. Furthermore, the change in lattice parameter will be smaller for the spinel than for the layered structure (Xia, Meng, et al., 2007). On the other hand, the activation barrier is also influenced by the change in effective valence of manganese ions with Li concentration. As seen with cyclic voltammetry, at around 4 V a small oxidation peak is present due to the Mn^{3+}/Mn^{4+} redox couple. When there are more or less the same numbers of Mn^{3+} and Mn^{4+} ions, the energy barrier will be the highest and it decreases again as there are more Mn^{4+} ions than Mn^{3+}. This means that Li ions are more favoured to be surrounded by Mn^{4+} ions, which can be attributed to the electrostatic effect. The electron clouds of Mn^{4+} ions are less dense than for Mn^{3+} ions, causing weaker Mn-O interactions for Mn^{3+} and thus longer Mn-O bond-lengths. As a consequence the Li-O bond-length will be shortened, leading to smaller Li 16c site octahedral volumes. So, Mn^{4+} ions enhance the ionic conductivity due to their smaller range of electron clouds. On the other hand, due to stronger coulombic repulsion, the Li^{+}-Mn^{4+} distances will be longer than the Li^{+}-Mn^{3+} distances. So, a larger amount of

Mn^{4+} ions may improve the ionic conductivity by lowering local Li diffusion activation barriers (W. W. Liu et al., 2017; Xu & Meng, 2010).

In Figure 6.8, one can also distinguish two minima, one at a potential of 4.69 V and one at around 4.76 V. These potentials are equal or very close to the potentials of the oxidation peaks identified with cyclic voltammetry. These oxidation peaks are related to the Ni^{2+}/Ni^{3+} and Ni^{3+}/Ni^{4+} redox couple. During charging the LNMO electrode undergoes two stages of phase change. $LiNi(II)_{0.5}Mn(IV)_{1.5}O_4$ changes to $Li_{0.5}Ni(III)_{0.5}Mn(IV)_{1.5}O_4$ and finally to $Ni(IV)_{0.5}Mn(IV)_{1.5}O_4$. The decrease in lithium diffusion coefficient is linked to the formation of phase boundaries which develop between phases during nucleation and growth processes in multiphasic electrodes. Because of a mismatch in lattice structure between phases, it becomes more difficult for lithium ions to diffuse (Rahim et al., 2022). However, when there is a two-phase region the measured lithium diffusion coefficient is actually an effective chemical diffusion coefficient. The effective chemical diffusion coefficient is a weighted average of the diffusivities in the different phases and the phase boundary (Springer & Lechner, 2005). This is because the lithium ion transport includes diffusion in two phases coupled to boundary kinetics, which means a single diffusion coefficient is not meaningful (Xia, Meng, et al., 2007).

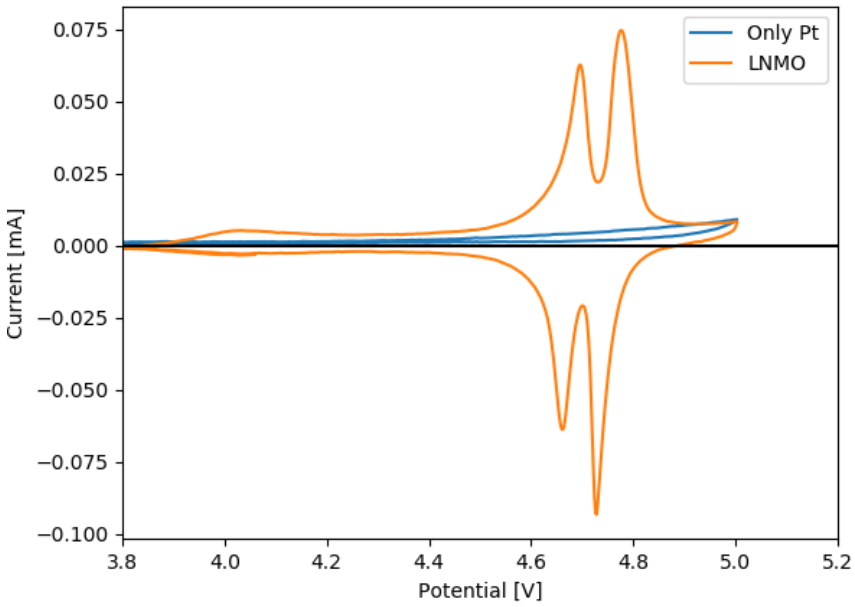

Figure 6.9: The comparison of a cyclic voltammetry experiment for a cell with pure Pt as working electrode and LNMO as working electrode. For both of them oxidation takes place at a potential above 4.8 V.

Towards the end of the charging process, at around 4.8 V, the potential starts to show peak-like behaviour (for the current pulse of 3 µA) as can be seen in Figure 6.5 b. This behaviour translates to a sudden drop in diffusion coefficient at a potential of over 4.8 V, as is shown in Figure 6.8. This could be because the electrolyte used ($LiPF_6$ in PC) is partially oxidized when the cell goes through the high voltage region, which forms a surface layer. This surface layer hinders the diffusion of lithium ions with a drop in diffusion coefficient as result (Xia et al.,

2009). In order to examine this, a cyclic voltammetry experiment was executed with platinum as working electrode. This way the reactions related to the LNMO material could be eliminated. The result is shown in Figure 6.9. For both Pt and LNMO as working electrode a rise in current is observed at a potential above 4.8 V, which means this oxidation is not related to LNMO. This is further proof the electrolyte starts partially oxidizing at high potentials vs. Li^+/Li.

6.3 PITT

For the Potentiostatic Intermittent Titration Technique (PITT) steps in potential are applied and the current response is measured. The steps applied must be small enough to fulfil the conditions. Therefore, the potential interval that needs to be crossed has to be divided by the size of the steps to find the number of cycles. In Figure 6.10 the current response to potential steps of 10 mV each applied for 4 minutes is shown. The potential ranges from 4.4 to 5 V, so in total there are 60 cycles. Each cycle is represented by a different color. The right figure represents a zoom in on the four first cycles. Every time the potential rises there is a sharp increase in current. During the four minutes the potential is held constant, the current relaxes again to an equilibrium value.

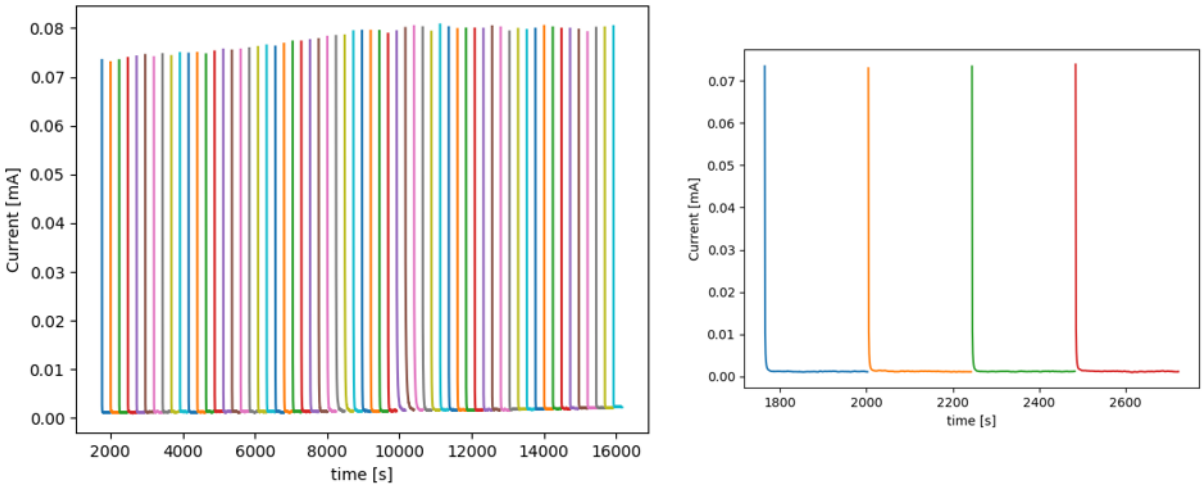

Figure 6.10: The current response to steps in potential of 10 mV each applied for a time of 4 minutes. The right figure shows a zoom in of the first four cycles.

From this data the evolution of the diffusion coefficient can be calculated. For PITT this can be done with two methods, on the one hand the long time method and on the other hand the short time method (or Cottrell analysis). For the long time method the time at which the calculation is done must be a lot longer than the diffusion time, $t >> L^2/\tilde{D}$. While for the short time method the time must be a lot shorter than the diffusion time, $t << L^2/\tilde{D}$. Other assumptions valid for both methods are the following: the variation of molar volume with composition must be negligible, diffusion must be the rate-determining process and prior to each step the material composition must be homogenized. These conditions are the same as for the GITT method. Both the long time and short time methods are described in the following sections.

6.3.1 Long time method

For PITT in most of literature the expression is used wherefore the time of the potential step must be a lot larger than the diffusion time ($t >> L^2/\tilde{D}$). The benefit of this method, is that one does not need to know the change in concentration or charge with the potential steps. The diffusion coefficient can be calculated using Equation 4.17.

When looking at Equation 4.17, the long time condition means that the slope of ln(I) vs. t must be taken at times longer than the diffusion time. In Figure 6.11 the window where the slope is taken is represented by a black line. By looking at this figure, one can see that for each potential step the logarithm of the current starts at a higher value. While the potential is held constant, the current first decreases rapidly. During this decrease the current relaxes until it reaches an equilibrium value. In the window where the slope is taken, full relaxation has taken place and the system is in steady state. This means there is no driving force for diffusion anymore. When looking at Figure 6.11, it becomes clear that the results for the diffusion coefficient using this slope, do not correspond with literature or the results obtained with GITT in the previous section. Instead of downward peaks the diffusion coefficient goes upwards during the oxidation of nickel (at potentials of 4.68 and 4.75 V). Furthermore, in the window where the slope is taken the data is very noisy, which translates to a noisier result for the evolution of the diffusion coefficient.

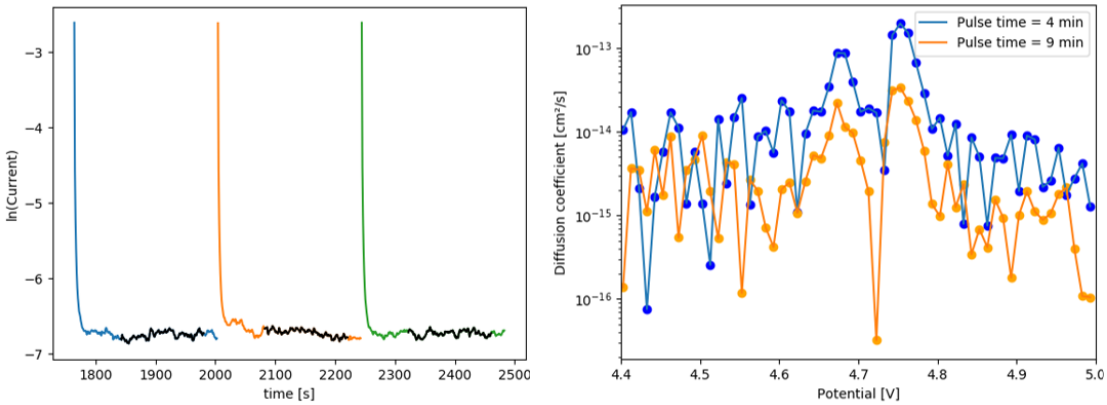

Figure 6.11: The ln(I) vs. t, the black line represents the window where the slope is taken for the calculation of the diffusion coefficient. Here the slope is taken at long times. In the right figure the diffusion coefficient calculated with this slope is given.

Figure 6.12 represents what the outcome is when the slope is taken at sooner times. The window where the slope is taken is represented by a black line. In this window the current is still relaxing towards a steady state. This means there is still a driving force for diffusion caused by the potential step. Here, the results for the diffusion coefficient match literature better. As can be seen in Figure 6.12, the peaks go downwards at potentials of 4.68 and 4.75 V, which is in correspondence with literature and the other techniques discussed in this thesis. However, now the condition of $t >> L^2/\tilde{D}$ is not met, which means Equation 4.17 is not valid and cannot be used.

It can be concluded that depending on where the slope is taken, the results for the diffusivity are very different. Furthermore, taking into account the condition valid for the long time method, one can say this method cannot be applied for thin film electrodes. This is because the condition means that the slope to calculate the diffusivity is taken where there is no influence of diffusion caused by the potential step anymore.

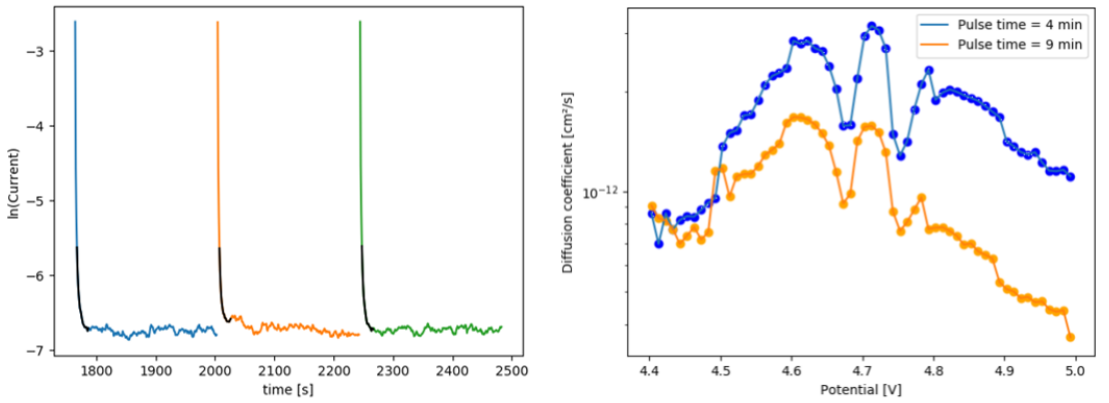

Figure 6.12: The ln(I) vs. t, the black line represents the window where the slope is taken for the calculation of the diffusion coefficient. Here the slope is taken at short times. In the right figure the diffusion coefficient calculated with this slope is given.

6.3.2 Short time method

As the method for long times is not valid, the method for short times should be used. The method for short times uses the Cottrell relationship, given in Equation 4.16. To determine the diffusion coefficient, the current must be plotted as a function of $1/\sqrt{t}$. By using the slope for each pulse, the evolution of the diffusion coefficient with potential can be established. For the short time method this slope must be taken early in the process.

The experiment wherefore the potential is applied in steps of 10 mV each for a time of 4 minutes will be discussed. The potential ranges from 3.8 to 5 V, which means there are 120 cycles. The window where the slope is taken can be seen in Figure 6.13 and is represented by a black line.

Unlike the method for long times, the slope is taken where the system is not in a steady state yet. The current is still relaxing towards an equilibrium value. This means there is still a driving force for diffusion caused by the potential step. Next to that, for the Cottrell analysis the condition that t has to be a lot smaller than the diffusion time ($t << L^2/\tilde{D}$) is met. Here, the slope is taken between 2 and 5 seconds after each step in potential.

The evolution of the diffusion coefficient obtained with the Cottrell relationship is depicted in Figure 6.14. The diffusion coefficient varies between 10^{-11} and 10^{-13} cm^2/s. As can be seen in Figure 6.14, the measurement of the diffusivity starts at a potential of 3.8 V and ends at a potential of 5 V. First the diffusivity decreases until it reaches a potential of around 4.3 V and then it starts increasing again. After that, two minima can be observed at potentials of 4.68 V and 4.75 V, with a local maximum in between. When a potential of around 4.8 V is reached, there is a slight decrease in diffusivity.

As for GITT the deflection point at around 4.3 V can be attributed to the oxidation of Mn^{3+} into Mn^{4+}. The activation barrier for Li-ion hopping reaches a maximum when there is more or less the same amount of Mn^{3+} and Mn^{4+} ions. When there is a majority of Mn^{4+} ions, it decreases again, as these ions hinder the diffusion of Li-ions less. Furthermore, the minima at 4.68 V and 4.75 V can be attributed to the oxidation of nickel. This corresponds to the peaks observed with cyclic voltammetry. However, as discussed before, the diffusion coefficient can only be seen as an effective diffusion coefficient here, since multiple processes are taking place at

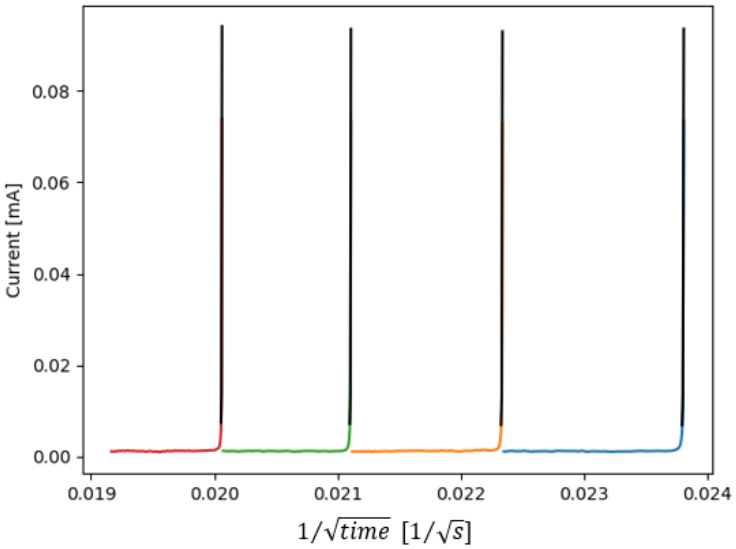

Figure 6.13: I vs. $1/\sqrt{t}$ for the four first pulses of a potential step of 10 mV. The black line represents the window where the slope is taken for the calculation of the diffusion coefficient. The slope is taken at short times.

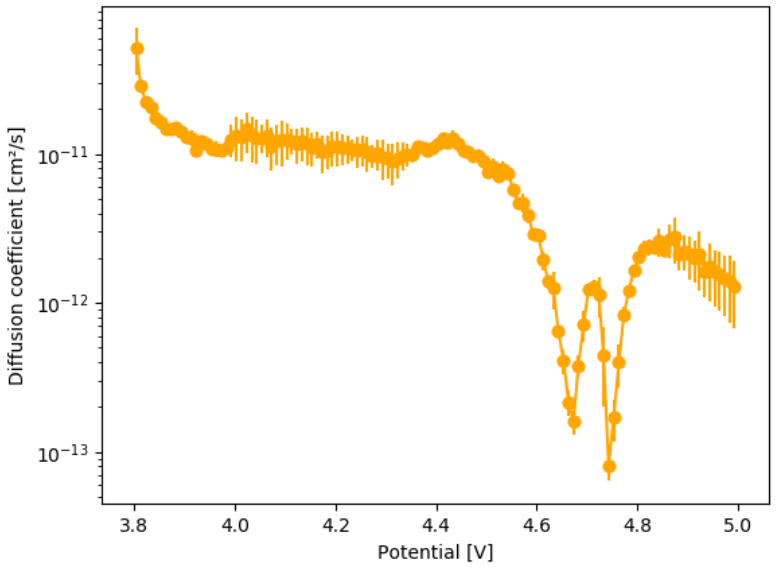

Figure 6.14: The evolution of the diffusion coefficient determined with the Cottrell relationship from a PITT experiment. The potential is applied in steps of 10 mV each time for 4 minutes.

once. At a potential of 4.71 V the diffusivity reaches a local maximum. It is expected that at this potential no phase transition is taking place anymore. At potentials higher than 4.8 V the decrease in diffusion coefficient can be attributed to the surface layer being formed because of partial oxidation of the electrolyte.

6.4 ICI

For ICI repeating current interruptions (usually 1 to 10 s) are introduced while the cell is under a constant-current. For the ICI technique the same assumptions are valid as for the GITT technique, except for the requirement of having to be in an equilibrium state. This is not necessary for ICI and thereby makes it a much faster technique.

To optimize the measurement of the diffusion coefficient using the intermittent current interruption technique different values for the current were tried out. The original idea was to charge with a constant-current C/2, with cycles of 5 minutes and interruptions of 10 seconds. The capacity of the LNMO samples is 1.37 µAh, so C/2 leads to a current of around 0.7 µA. Applying 0.7 µA for 2 hours in steps of 5 minutes means one needs 24 steps. Taking into account the discharge during the interruptions, 30 steps were applied. However, with this current of 0.7 µA for 30 cycles a potential of only 4.66 V was reached, which is not enough to distinguish the reactions happening at potentials of 4.69 and 4.77 V. This could be explained based on side reactions taking place in the high-voltage region. Therefore, the applied current was gradually increased. For a current of 1.5 µA a potential of 4.9 to 5 V could be reached.

In Figure 6.15 the potential response as a function of time is given for a current of 1.5 µA. This shows an upward trend in potential with time. Between 4.6 V and 4.7 V the potential stabilizes for a first time. Between 4.75 V and 4.8 V it stabilizes a second time. When reaching a potential of 4.95 V, the drops in potential during the current interruptions become larger. In Figure 6.15 a zoom in of the first two cycles is shown as well, to have a better view of what happens during each sequence. The expected behaviour can be distinguished. There is a continuous increase in potential except for the periods during which the current is interrupted where the potential decreases.

In Figure 6.16 the potential is plotted as a function of $\sqrt{time}$ for the 15^{th} cycle of the ICI experiment. This 15^{th} cycle is taken to give an example, but for the other cycles the result is similar. The black color represents the window where the slope is taken. Since the current is only interrupted for 10 seconds this window is a lot more limited than for GITT and PITT. This makes it easier to decide where to take the interval to determine the slope. However, as can be seen in Figure 6.16 the potential response is very noisy, which also translates to a noisier result for the diffusivity.

The evolution of the diffusion coefficient obtained with the ICI technique is given in Figure 6.17. As can be seen in Figure 6.17 the diffusivity varies between 10^{-9} and 10^{-13}. It is measured for a potential starting from 4.2 V and ending at a potential a little higher than 4.9 V. First the diffusion coefficient decreases until it reaches a potential of around 4.3 V, then it increases again. Two minima in diffusivity are observed at around 4.69 V and 4.76 V, with in between a local maximum. For potentials higher than 4.8 V the diffusivity decreases. When comparing this to GITT and PITT, the same trends in evolution of the diffusion coefficient are visible. The deflection point around 4.3 V can again be attributed to the Mn^{3+}/Mn^{4+} redox couple. The drops in diffusion coefficient at 4.69 V and 4.76 V correspond to the phase transitions happening during the oxidation of nickel. At this point the diffusion coefficient includes the diffusion in multiple phases and boundary kinetics, so actually it is the effective diffusion coefficient. The decrease in diffusion coefficient at potentials higher than 4.8 V also comes back in Figure 6.15.

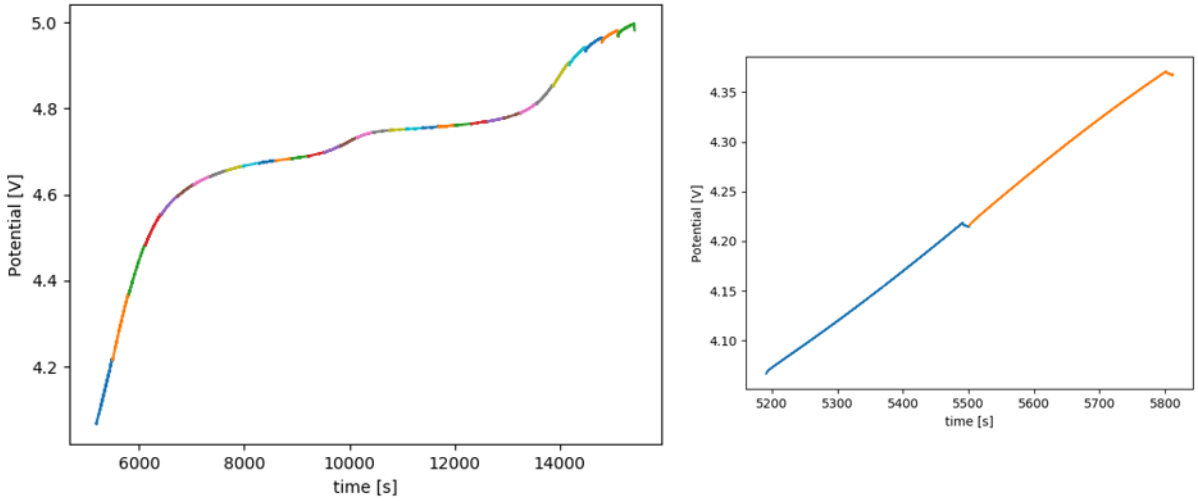

Figure 6.15: The potential response as a function of time for a current of 1.5 µA applied during 5 minutes with interruptions of 10 seconds for each cycle. The right figure shows a zoom in on the first two cycles.

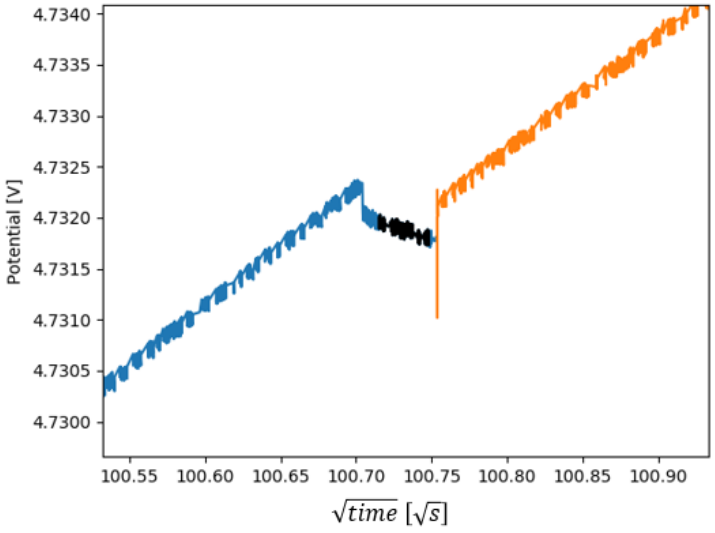

Figure 6.16: The potential is plotted as a function of $\sqrt{time}$ for the 15^{th} cycle. The black line represents the window where the slope is taken.

As mentioned before, at around 4.95 V the potential response as as a function of time changes to more peak-like behaviour. This can, like with GITT and PITT, be related to the formation of a surface layer with the partial oxidation of the electrolyte.

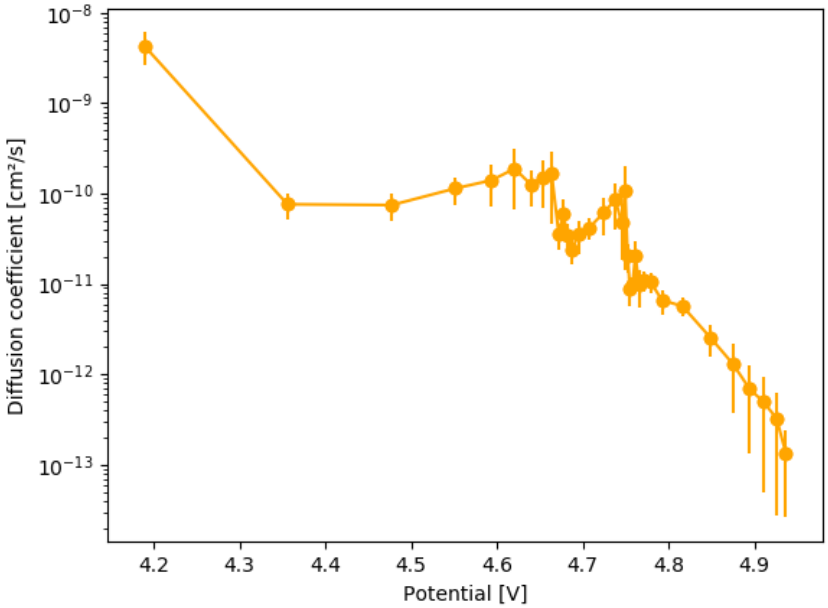

Figure 6.17: The evolution of the diffusion coefficient obtained with the ICI technique (with a current of 1.5 µA).

6.4.1 Comparison different electrode thicknesses

As ICI is the fastest technique out of the three, it was used to try establish the influence of electrode thickness on the diffusivity. Besides a thickness of 70 nm, the ICI technique was also applied on electrodes with a thickness of 210 and 280 nm. The same conditions were used for all of them: a current of 1.5 µA applied for 5 minutes with interruptions of 10 seconds repeated 60 times.

The potential response as a function of time is given in Figure 6.18. This Figure shows that with increasing thickness the potential stabilizes at a decreasing value. This could be expected as there is a decrease in current per unit of volume for increasing thickness of the electrode. This means a higher current would have to be applied with increasing thickness to be able to compare the diffusivity for different electrode thicknesses using ICI. However, due to insufficient time this could not be elaborated more.

6.5 Comparison of different techniques

In Figure 6.19 the evolution of the diffusion coefficient obtained with the 3 techniques are compared to each other.

The biggest difference between the three methods is the order of magnitude of the diffusivity. ICI shows the highest order of magnitude with a variation between 10^{-9} and 10^{-13} cm²/s. Then for PITT the diffusion coefficient varies from 10^{-11} to 10^{-13} cm²/s. For GITT it goes from 10^{-13} to 10^{-15} cm²/s. For PITT steps in potential are applied and the current response is measured, while for GITT and ICI current pulses are applied and the potential response is measured. The

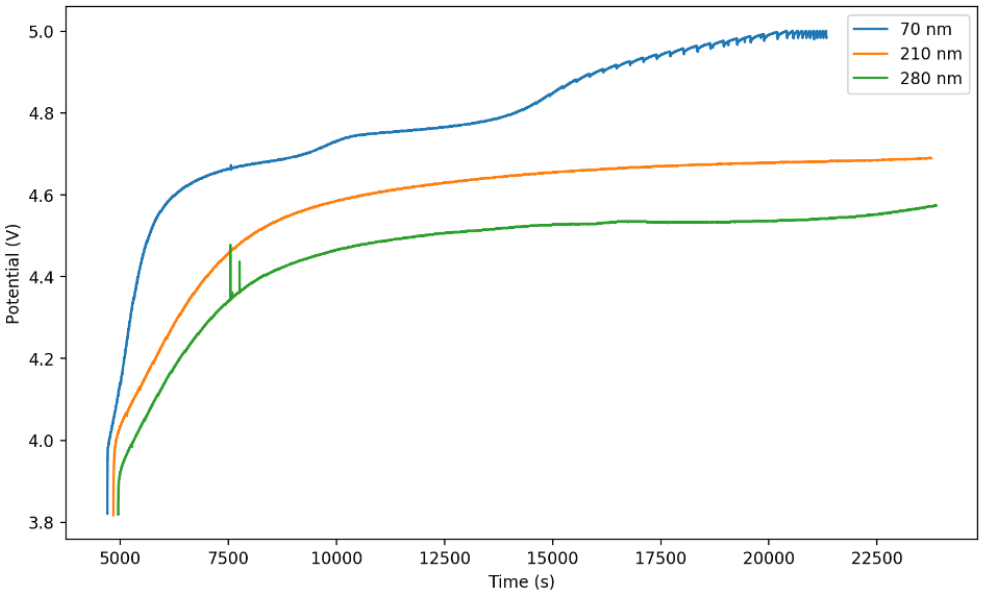

Figure 6.18: The potential response as a function of time for thin film electrodes with a thickness of 70, 210 and 280 nm.

difference in order of magnitude between the three methods points out that depending on what is applied (a current or a potential) the response will be different. As the ICI technique is deviated from GITT, the difference between both can only come from the value for the slope (E vs. $\sqrt{time}$) or the change in steady-state voltage for each cycle. When comparing the third factor in Equation 4.8 it becomes clear that its value is larger for ICI than for GITT. This is mainly due to the slopes, which are less steep for ICI compared to GITT. For GITT the slope is taken during the current pulse, while for ICI the slope is taken during the current interruption. This means the potential increases more rapidly when applying a current than that it decreases during relaxation. By using thin films, it was expected that the difference in diffusivity between the different techniques would be smaller compared to what is seen in literature for composite electrodes. However, that is not the case. This means that the difference is based on a physical phenomenon taking place during delithiation, that is different depending on the technique used. The reason for this must be further investigated in the future.

Furthermore, all three methods show similar trends. First of all, a deflection point in diffusivity at around 4.3 V is observed for all of them. This is related to the oxidation of Mn^{3+} into Mn^{4+} and corresponds to the peak observed with cyclic voltammetry at around 4 V. Secondly, two minima can be observed around the potentials associated to the oxidation of nickel. However, the three techniques used in this work are based on classical Fickian dynamics, with no gradient free energy term (Han et al., 2004). For phase transitions taking place during nickel oxidation, the Li-ion transport includes diffusion in two phases coupled to boundary kinetics, which means a single diffusion coefficient is not meaningful. So, around these oxidation potentials one should speak of the effective diffusion coefficient. In between these minima there is a maximum that goes back to the original diffusivity (from before the first minimum). One can conclude that at the potential corresponding to this maximum there is no phase transition anymore and this can be taken as the real diffusivity. Next to that, for all three of the techniques the diffusion

coefficient goes down when reaching a potential of 4.8 V corresponding to the formation of the surface layer with partial electrolyte oxidation. For GITT and ICI this drop goes more rapidly than for PITT. This means that for GITT and ICI in the high-potential window, most of the applied current goes to side reactions instead of charging of the battery.

When comparing GITT to PITT there is a small shift in the position of the first minimum and maximum. For PITT this already takes place at lower potential compared to GITT. In general GITT is considered as more reliable than PITT in the phase-transition area. This can be explained based on the fact that with PITT potential steps are applied, which forces the potential to increase with a certain amount. In the vicinity of the phase transition this forms a problem, since the steps taken can be too big (Markevich et al., 2005).

When looking at Figure 6.19 the ICI technique shows the biggest error bars. This is related to the data from which the diffusion coefficient is deduced, being more noisy. As the current is interrupted for only 10 seconds, the potential only changes a little in the window where the slope is taken (in the order of 10^{-4} V), which decreases the signal-to-noise ratio. Based on this, one can say GITT and PITT are more reliable to determine the diffusivity for thin film electrodes. Furthermore, the diffusion coefficient decreases more rapidly for the methods based on a potential response (GITT and ICI) than for the method based on a current response (PITT) in the high-voltage region. As mentioned before, this is because of the applied current going to side reactions, instead of charging the battery. Based on this, even though PITT depends on where the slope is taken, it proves to be more reliable for the determination of the diffusion coefficient of positive electrode thin films at high potentials.

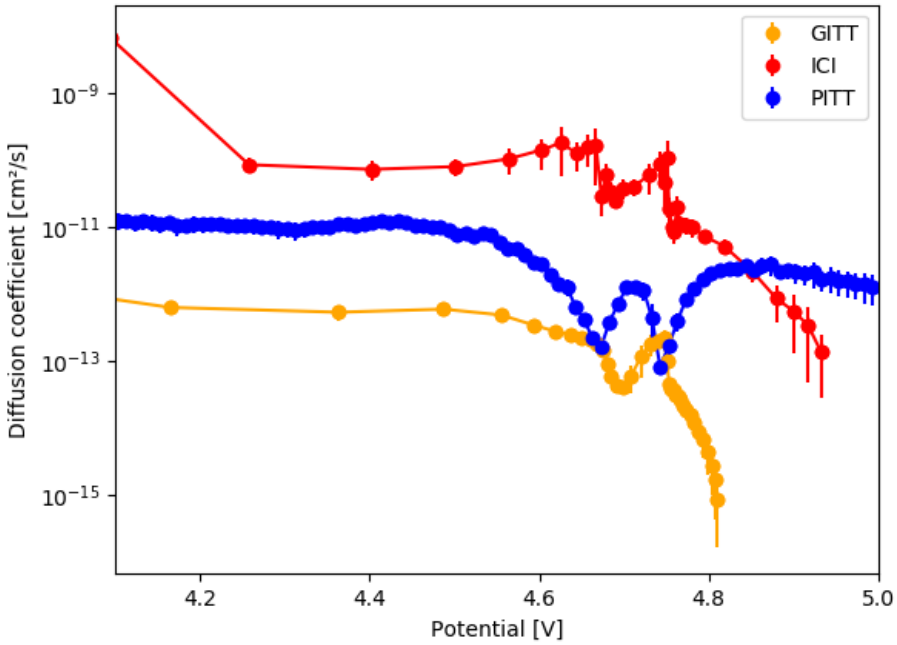

Figure 6.19: The evolution of the diffusion coefficient obtained with GITT, PITT and ICI.

6.6 Comparison to literature

In this section the results for the diffusion coefficient obtained in this study are compared to those in literature. This is done for both GITT and PITT. For ICI this could not be done as this is a relatively new technique and it has not been implemented on LNMO electrodes in literature yet.

6.6.1 GITT

The evolution of diffusion coefficient found back in literature, using the GITT technique, is given in Figure 6.20. In literature the LNMO positive electrode material is synthesized by the sol gel method (while in this work sputtering is used). The potivive electrode exists out of 80 wt% LNMO, 10 wt% poly(vinylidene fluoride) (PVDF) binder, 10 wt% acetylene black and an aluminium foil current collector. The thickness of the composite electrode is 25 µm. The advantage of using thin film electrodes is their sufficient electric conductivity because of which no binders or additives are needed. The electrolyte used in the cells is 1 M $LiPF_6$ in an equal volume mixture of ethylene carbonate (EC) and dimethyl carbonate (DMC). In this study the electrolyte used is 1 M $LiPF_6$ in propylene carbonate (PC). For the application of the GITT technique current pulses of 34 µA are applied for 10 minutes with relaxation times of 40 minutes in between (Rahim et al., 2022).

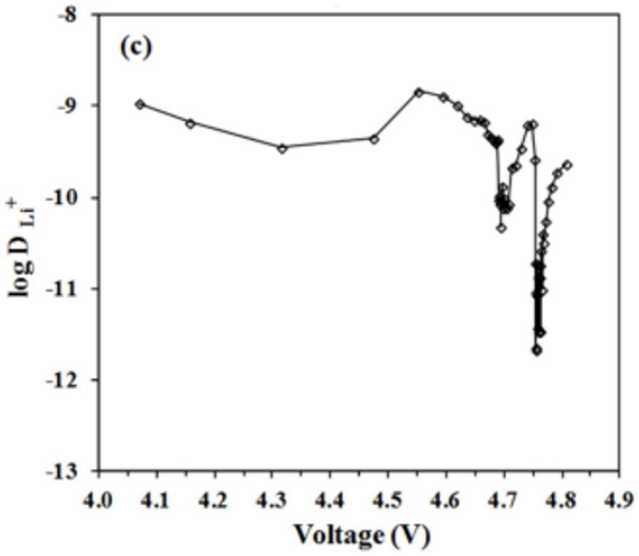

Figure 6.20: The evolution of the diffusion coefficient obtained with the GITT technique (Rahim et al., 2022).

Due to many variables being involved, it becomes difficult to determine intrinsic properties of the active material in composite electrodes. Since thin film electrodes have well-defined geometries and pure active materials they are ideal samples to study the intrinsic properties of electrode materials (Xia et al., 2009). So, the obtained values for the diffusion coefficient will be different compared to those for composite electrodes. This is due to the absence of conductive additives and binders, but also due to the well-defined geometric surface area. In composite electrodes the permeation of electrolyte through the additives into the active material augments

the contact area during the intercalation/deintercalation process. So, the determination of total contact area between the electrolyte and active material is nearly impossible. While, for the thin film electrodes this contact area can be approximated to the thin film surface since a smooth and dense thin film surface can be obtained (Shi et al., 2010; Xia et al., 2009). In this study this surface area is 0.785 cm^2.

When comparing the result from this study (Figure 6.8) with the result from literature the main difference lies in the order of magnitude. In Figure 6.20 the diffusivity varies from 10^{-9} to 10^{-12} cm^2/s, while in this study it goes from 10^{-12} to 10^{-15} cm^2/s for GITT. This difference can partly be attributed to the geometric surface area that is not as easy to define for composite electrodes. Next to that the observed trends are very similar. In literature one can also distinguish a deflection point at around 4.3 V and two downward peaks at 4.7 and 4.75 V. Furthermore, a local maximum can be found around 4.74 V in Figure 6.20, which is also the case for the result obtained in this study. However, in literature the diffusion coefficient does show an upward evolution after the second minimum. This means that for the cell in literature, if partial oxidation of the electrolyte takes place, its influence is a lot smaller. This can be explained based on the fact that the electrode in literature is a composite electrode with a thickness in the range of µm (25 µm to be exact) instead of nm as for thin films. Because of this larger thickness the surface effects become smaller compared to what happens in the bulk of the electrode and will have less of an impact.

6.6.2 PITT

The evolution of the diffusion coefficient found back in literature, using the PITT technique, is given in Figure 6.21. Figure (a) represents the diffusion coefficient for a $LiNi_{0.5}Mn_{1.5}O_4$ thin film electrode, while figure (b) represents a composite electrode.

The LNMO thin films are deposited on stainless steel substrates by pulsed laser deposition. The electrochemical cell exists out of a Li-metal foil counter electrode, a $LiNi_{0.5}Mn_{1.5}O_4$ thin film working electrode with an active area of around 0.785 cm^2, and 1 M $LiPF_6$ in EC/DEC (1/1 vol%) as the electrolyte. The thin film working electrode has a thickness that is estimated to be about 500 nm. To measure the diffusion coefficient the potentiostatic intermittent titration technique was used with a potential step of 10 mV. When the current dropped below 0.1 $\mu A/cm^2$, the potential was stepped to the next level. This procedure was repeated between 4.50 and 4.90 V. The diffusivity was extracted from the current response using the Cottrell analysis (Xia, Meng, et al., 2007).

The composite electrode exists out of 88 wt% LNMO, 4 wt% graphite, 2 wt% carbon black and 6 wt% polyvinylidene fluoride (PVdF) acting as binder. This electrode has a circular disk form with a diameter of 12 mm. In the electrochemical cell the coin cell with LNMO is used as the positive electrode and lithium metal foil as the negative electrode. For the electrolyte a mixture of ethylene carbonate (EC) and dimethyl carbonate (DMC) (EC:DMC = 1/2 vol%) solvents containing 1 M $LiPF_6$ was used. In the PITT measurements a potential step of 30 mV was applied after the electrode reached equilibrium which was evaluated by a current of less than 1 µA, this was repeated between 4.4 and 4.9 V. The diffusivity was extracted from the current response using the long time method. As characteristic diffusion length (L in Equation 4.17), the thickness of the electrode was used (M. H. Liu et al., 2014).

For the thin film electrode the value of the diffusivity varies between 10^{-10} and 10^{-12} cm^2/s. For the composite electrode the order of magnitude is lower and varies between 10^{-13} and 10^{-15} cm^2/s. Two minima at around 4.69 and 4.75 V can be observed, corresponding to the oxidation of nickel, respectively Ni^{2+} to Ni^{3+} and Ni^{3+} to Ni^{4+}. When going to a lower potential than 4.69

V and a higher potential than 4.75 V the diffusion coefficient shows an upward trend. Between both minima the diffusion coefficient reaches a local maximum at around 4.7 V.

When comparing this to the outcome obtained with PITT in this thesis (Figure 6.14) there are some similarities and some differences. First of all, the diffusivity varies between 10^{-11} and 10^{-13} cm^2/s, which lies between the orders of magnitude found for the thin film and composite electrode in literature. As noticed in the analysis of the diffusivity in this work, the outcome depends a lot on where the slope (ln(I) vs. t or I vs. $\sqrt{t}$) is taken. This can explain why there is such a difference in orders of magnitude for the diffusion coefficient between different references and this study. Next to that, one can also observe a local maximum around 4.7 V and minima at 4.68 and 4.75 V. Furthermore, the diffusivity does increase below 4.67 V and above 4.75 V. However, for potentials lower than 4.67 V the diffusion coefficient decreases slightly starting from 4.4 V to lower potentials and then stabilizes to a value around 10^{-11}. This decrease is attributed to the manganese oxidation and comes back for the composite electrode in literature. Above 4.79 V it reaches a local maximum at around 4.8 V. The decrease in diffusion coefficient above this potential can be explained based on the partial oxidation of the electrolyte. This trend comes back for the thin film electrode in literature, but not for the composite electrode. The reason for it not being visible for composite electrodes is the same as discussed for composite electrodes in GITT.

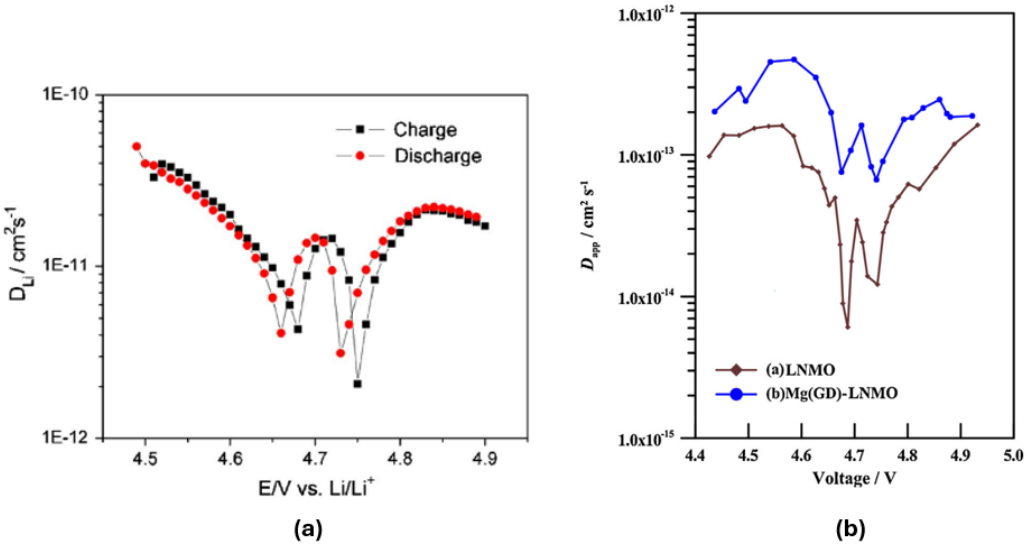

Figure 6.21: The evolution of the diffusion coefficient obtained with the PITT technique (a) thin film LNMO electrode (Xia, Meng, et al., 2007) and (b) composite LNMO electrode (M. H. Liu et al., 2014).

Conclusion

To model the optimal design for a battery containing LNMO as positive electrode, a reliable, quantitative description of the lithium diffusion coefficient is needed. In literature there is still a large variation in order of magnitudes for this diffusion coefficient, on the one hand between different techniques used and on the other hand for the same technique between different references. By using thin film LNMO electrodes instead of composite electrodes, it was expected that the difference in value for the diffusivity obtained with different techniques would decrease. In this thesis three electrochemical methods were developed: GITT, PITT and ICI.

So, the objectives of this thesis are firstly to validate if using thin film electrodes indeed makes the difference in outcome for the three techniques smaller. Secondly, the evolution of the diffusion coefficient with potential should be described. Thirdly, the most reliable method out of the three should be attempted to be identified. Finally, it should be examined if the thickness of the thin film electrodes has an influence on their electrochemical behaviour.

First, the difference in order of magnitude between the different methods will be discussed. Even when using thin film electrodes the difference in order of magnitude between the three techniques remains. The diffusivity varies between 10^{-9} and 10^{-13} cm^2/s for ICI, between 10^{-11} and 10^{-13} cm^2/s for PITT and between 10^{-13} and 10^{-15} cm^2/s for GITT. Even though ICI is developed starting from GITT, the resulting order of magnitude is very different. For ICI the data from which the diffusivity is derived, is very noisy. The potential only changes in the order of 10^{-4} V in the window where the slope is taken to calculate the diffusivity, which decreases the signal-to-noise ratio. This makes ICI less reliable to determine the diffusion coefficient for thin film electrodes. The difference in order of magnitude between GITT and PITT can only be attributed to the difference in what is applied and what is measured. For GITT a current pulse is applied and the potential response is measured, while for PITT potential steps are applied and the current response is measured. The physical reason behind the difference in value obtained for the lithium diffusion coefficient using the three techniques is still unclear. Therefore, further investigation is necessary.

Secondly, the evolution of the diffusion coefficient is described. The three methods show a similar trend in evolution of the diffusion coefficient. First, there is a decrease and then again an increase in diffusivity in the low-potential window with a deflection point at around 4.3 V. This can be attributed to the activation barrier for Li-ions to jump that first slightly increases and then decreases again. This diffusion activation barrier is the energy difference between lithium's initial tetrahedral 8a state and the metastable empty octahedral 16c state that it passes when going to another 8a state. The activation barrier is influenced by the change in effective valance of manganese ions with lithium concentration. As seen with cyclic voltammetry, around 4 V there is an oxidation peak related to the Mn^{3+}/Mn^{4+} redox couple. When there are more or less the same amount of Mn^{3+} and Mn^{4+} ions the energy barrier will be the highest. It decreases

again with increasing amount of Mn^{4+} ions. This is because of their smaller range of electron clouds and stronger coulombic repulsion making the Li^{+}-Mn^{4+} distances longer.

When going to higher potentials all of the techniques show two minima at around 4.7 and 4.75 V corresponding to the Ni^{2+}/Ni^{3+} and Ni^{3+}/Ni^{4+} redox couples. These potentials again correspond to what was seen with cyclic voltammetry. During charging the LNMO electrode undergoes two stages of phase transition: $LiNi(II)_{0.5}Mn(IV)_{1.5}O_4$ changes to $Li_{0.5}Ni(III)_{0.5}Mn(IV)_{1.5}O_4$ and finally to $Ni(IV)_{0.5}Mn(IV)_{1.5}O_4$. However, when there is a two-phase region the measured lithium diffusion coefficient is an effective chemical diffusion coefficient. This is because the lithium ion transport includes diffusion in two phases coupled to boundary kinetics, which means a single diffusion coefficient is not meaningful. Between these two minima there is a local maximum at around 4.74 V for GITT and ICI and at 4.71 V for PITT, wherefore the diffusivity goes back to its value from before the first minimum. At this potential there is no phase transition anymore and this can be taken as the real diffusion coefficient.

At around 4.8 V there is a decrease in diffusion coefficient for all of the techniques. This is assigned to the partial oxidation of the electrolyte ($LiPF_6$ in PC) when the cell goes through the high voltage region. This partial oxidation of the electrolyte creates a surface layer, making Li-ion diffusion through the electrode a lot harder. Next to that, the applied current (in the case of GITT and ICI) is used more for these side-reactions than for charging the battery.

Thirdly, by comparing the three methods, it was possible to establish the most reliable one. As mentioned before, the diffusivity obtained with ICI shows the biggest error bars, which is related to the data from which the diffusion coefficient is deduced, being more noisy. Furthermore, the diffusion coefficient decreases more rapidly for the methods based on a potential response (GITT and ICI) than for the method based on a current response (PITT) in the high-voltage region. This is because the applied current is going to the side reactions taking place instead of charging the battery. Based on this, even though PITT depends on where the slope is taken, it proves to be more reliable for the determination of the diffusion coefficient of the positive electrode thin films at high potentials.

Lastly, the investigation on influence of the thickness of thin film electrodes was started. A change in behaviour is observed starting from a thickness of around 200 nm. More specifically, with cyclic voltammetry the ratio of the height of the peaks corresponding to nickel oxidation changed. Furthermore, when trying to determine the diffusion coefficient for the different thicknesses using ICI, a decrease in final stabilized potential with increasing thickness was discovered. This was expected, since the current per unit of volume decreases with increasing thickness of the electrode. However, due to insufficient time this could not be elaborated more.

In summary, even when using thin film electrodes the difference in order of magnitude in diffusion coefficient obtained with GITT, PITT and ICI remains. It is still unclear what the physical reason is behind this difference. Therefore, further investigation should be done. However, all three methods do show a similar trend in the evolution of the diffusivity. Furthermore, it is established that PITT is the preferred technique to determine the diffusion coefficient in thin film electrodes. Finally, a start in exploring the influence of thin film electrode thickness was done. More research on this should be done in the future.

Future work

In future work the reason for the difference in order of magnitude between the diffusion coefficients obtained with GITT, PITT and ICI should be further investigated. This could be done using Electrochemical Impedance Spectroscopy (EIS). EIS could give more insights on the correct determination of the diffusion coefficient in thin film systems. This is because EIS goes to the frequency domain, while GITT, PITT and ICI stay in the time domain. By going to the frequency domain it might be possible to have a better separation of the diffusion phenomena from the complex reactions taking place in the LNMO material. Another way is to introduce the different orders of magnitude in the model and study how they influence the outcome. By doing this one might get a better idea of what causes the difference between the three methods on a physical level.

Something else worth researching in more depth is the effect of the thickness of the thin film electrode on the determination of the diffusivity. As observed with cyclic voltammetry, around a thickness of 200 nm the behaviour around the nickel redox couples changes. More specifically, the peak at a lower potential becomes larger than the one at a higher potential. So, it should be studied what causes this change. Next to that, the influence of the electrode thickness on the diffusivity should also be investigated, using the different methods described in this work.

Bibliography

Aktaş, A., & Kirçiçek, Y. (2021). Solar hybrid systems. In *Solar hybrid systems* (pp. 111–120). Academic Press.

Amin, R., & Belharouk, I. (2017). Part i: Electronic and ionic transport properties of the ordered and disordered $LiNi_{0.5}Mn_{1.5}O_4$ spinel cathode. *Journal of Power Sources*, *348*, 311–317. https://doi.org/10.1016/j.jpowsour.2017.02.071

Amin, R., Muralidharan, N., Petla, R. K., Yahia, H. B., Al-Hail, S. A. J., Essehli, R., & Belharouak, I. (2020). Research advances on cobalt-free cathodes for Li-ion batteries-the high voltage $LiMn_{1.5}Ni_{0.5}O_4$ as an example. *Journal of Power Sources*, *467*. https://doi.org/10.1016/j.jpowsour.2020.228318

Amiryar, M. E., & Pullen, K. R. (2017). A review of flywheel energy storage system technologies and their applications. *Applied Sciences*, *7*(3), 286. https://doi.org/10.3390/app7030286

Babu, B. (2024). Self-discharge in rechargeable electrochemical energy storage devices. *Energy Storage Materials*, *103261*. https://doi.org/10.1016/j.ensm.2024.103261

Bhatia, A., Zrelli, Y. D., Pereira-Ramos, J. P., & Baddour-Hadjean, R. (2021). Detailed redox mechanism and self-discharge diagnostic of 4.9 V $LiMn_{1.5}Ni_{0.5}O_4$ spinel cathode revealed by Raman spectroscopy. *Journal of Materials Chemistry A*, *9*(23), 13496–13505. https://doi.org/10.1039/D1TA90125G

Bhattacharya, J., & Van der Ven, A. (2010). Phase stability and nondilute Li diffusion in spinel $Li_{1+x}Ti_2O_4$. *Physical Review B*, *81*(10). https://doi.org/10.1103/PhysRevB.81.104304

Brett, C. M. A., & Brett, A. M. O. (1993). *Electrochemistry—principles, methods, and applications*. Oxford University Press.

Chen, S., Xiong, J., Qiu, Y., Zhao, Y., & Chen, S. (2023). A bibliometric analysis of lithium-ion batteries in electric vehicles. *Journal of Energy Storage*, *63*. https://doi.org/10.1016/j.est.2023.107109

Chien, Y. C., Liu, H., Menon, A. S., Brant, W. R., Brandell, D., & Lacey, M. J. (2021). A fast alternative to the galvanostatic intermittent titration technique. https://doi.org/10.26434/chemrxiv-2021-09srz

Chien, Y. C., Liu, H., Menon, A. S., Brant, W. R., Brandell, D., & Lacey, M. J. (2023). Rapid determination of solid-state diffusion coefficients in Li-based batteries via intermittent current interruption method. *Nature Communications*, *14*(1). https://doi.org/10.1038/s41467-023-37989-6

De Decker, K. (2020). Ditch the batteries: Off-grid compressed air energy storage. *Low-Tech Magazine*.

Energy Education. (n.d.). *Power density* [Accessed: April 4, 2024]. https://energyeducation.ca/encyclopedia/Power_density#cite_note-1

EV Express. (n.d.). Lithium ion battery [Accessed: May 23, 2024]. https://www.evexpress.net/Li-Ion.html

Geng, Z., Chien, Y. C., Lacey, M. J., Thiringer, T., & Brandell, D. (2022). Validity of solid-state Li^+ diffusion coefficient estimation by electrochemical approaches for lithium-ion batteries. *Electrochimica Acta*, *404*. https://doi.org/10.1016/j.electacta.2021.139727

Gourley, S. W. D., Or, T., & Chen, Z. (2020). Breaking free from cobalt reliance in lithium-ion batteries. *iScience*. https://doi.org/10.1016/j.isci.2020.101505

Han, B. C., Van der Ven, A., Morgan, D., & Ceder, G. (2004). Electrochemical modeling of intercalation processes with phase field models. *Electrochimica Acta*, *49*(26), 4691–4699. https://doi.org/10.1016/j.electacta.2004.05.024

Hausbrand, R., Cherkashinin, G., Ehrenberg, H., Gröting, M., Albe, K., Hess, C., & Jaegermann, W. (2015). Fundamental degradation mechanisms of layered oxide li-ion battery cathode materials: Methodology, insights and novel approaches. *Materials Science and Engineering: B*, *192*, 3–25. https://doi.org/10.1016/j.mseb.2014.11.014

Hirscher, M., Yartys, V. A., Baricco, M., von Colbe, J. B., Blanchard, D., Bowman Jr, R. C., & Zlotea, C. (2020). Materials for hydrogen-based energy storage–past, recent progress and future outlook. *Journal of Alloys and Compounds*, *827*, 153548. https://doi.org/10.1016/j.jallcom.2019.153548

Hubin, A. (2021). *Electrochemistry: Fundamentals and applications*.

Intergovernmental Panel on Climate Change. (2023). *Climate change 2023: Synthesis report* [Summary for Policymakers].

Kang, S. D., & Chueh, W. C. (2021). Galvanostatic intermittent titration technique reinvented: Part i. a critical review. *Journal of The Electrochemical Society*, *168*(12). https://doi.org/10.1149/1945-7111/ac3940

Kim, J. H., Myung, S. T., Yoon, C. S., Kang, S. G., & Sun, Y. K. (2004). Comparative study of $LiNi_{0.5}Mn_{1.5}O_{4-\delta}$ and $LiNi_{0.5}Mn_{1.5}O_4$ cathodes having two crystallographic structures: Fd-3m and P4332. *Chemistry of materials*, *16*(5), 906–914. https://doi.org/10.1021/cm035050s

Korthauer, R. (2018). *Lithium-ion batteries: Basics and applications*. Springer.

Kulova, T. L., Fateev, V. N., Seregina, E. A., & Grigoriev, A. S. (2020). A brief review of post-lithium-ion batteries. *International Journal of Electrochemical Science*, 7242–7259. https://doi.org/10.20964/2020.08.22

Liu, M. H., Huang, H. T., Lin, C. M., Chen, J. M., & Liao, S. C. (2014). Mg gradient-doped $LiNi_{0.5}Mn_{1.5}O_4$ as the cathode material for Li-ion batteries. *Electrochimica Acta*, *120*, 133–139. https://doi.org/10.1016/j.electacta.2013.12.065

Liu, W., Shi, Q., Qu, Q., Gao, T., Zhu, G., Shao, J., & Zheng, H. (2017). Improved Li-ion diffusion and stability of a $LiNi_{0.5}Mn_{1.5}O_4$ cathode through in situ co-doping with dual-metal cations and incorporation of a superionic conductor. *Journal of Materials Chemistry A*, *5*(1), 145–154. https://doi.org/10.1039/c6ta08891k

Liu, W. W., Wang, D., Wang, Z., Deng, J., Lau, W. M., & Zhang, Y. (2017). Influence of magnetic ordering and jahn–teller distortion on the lithiation process of $LiMn_2O_4$. *Physical Chemistry Chemical Physics*, *19*(9), 6481–6486. https://doi.org/10.1039/c6cp08324b

Manthiram, A. (2020). A reflection on lithium-ion battery cathode chemistry. *Nature communications*, *11*(1). https://doi.org/10.1038/s41467-020-15355-0

Markevich, E., Levi, M., & Aurbach, D. (2005). Comparison between potentiostatic and galvanostatic intermittent titration techniques for determination of chemical diffusion coefficients in ion-insertion electrodes. *Journal of Electroanalytical Chemistry*, *580*(2), 231–237. https://doi.org/doi.org/10.1016/j.jelechem.2005.03.030

Megahed, S., & Scrosati, B. (1994). Lithium-ion rechargeable batteries. *Journal of Power Sources*, *51*(1-2), 79–104. https://doi.org/10.1016/0378-7753(94)01956-8

Mehrer, H. (2007). *Diffusion in solids: Fundamentals, methods, materials, diffusion-controlled processes*. Springer.

MIT Electric Vehicle Team. (2008). A guide to understanding battery specifications [Accessed: May 23, 2024]. https://web.mit.edu/evt/summary_battery_specifications.pdf

Mohamed, N. M., & Allam, N. K. (2020). Recent advances in the design of cathode materials for Li-ion batteries. *RSC Advances*, *10*(37), 21662–21685. https://doi.org/10.1039/d0ra03314f

Montella, C. (2002). Discussion of the potential step method for the determination of the diffusion coefficients of guest species in host materials: Part i. influence of charge transfer kinetics and ohmic potential drop. *Journal of Electroanalytical Chemistry*, *518*(2), 61–83. https://doi.org/10.1016/S0022-0728(01)00691-X

Murer, N., Diard, J.-P., & Petrescu, B. (2021). Determination of the diffusion coefficient of an inserted species in a host electrode with EIS, PITT and GITT techniques. https://doi.org/10.13140/RG.2.2.34491.13605

Naskar, P., Debnath, S., Mukherjee, N., & Banerjee, A. (2023). Indispensable assets for rechargeable world: Lithium-ion batteries. *Resonance*, *28*(4), 577–596. https://doi.org/10.1007/s12045-023-1584-6

Nikitina, V. A. (2020). Charge transfer processes in the course of metal-ion electrochemical intercalation. *Current Opinion in Electrochemistry*, *19*, 71–77. https://doi.org/10.1016/j.coelec.2019.10.006

Population. (n.d.). United Nations. https://www.un.org/en/global-issues/population

Rahim, A. S. A., Kufian, M. Z., Arof, A. K. M., & Osman, Z. (2022). Variation of Li diffusion coefficient during delithiation of spinel $LiNi_{0.5}Mn_{1.5}O_4$. *Journal of Electrochemical Science and Technology*, *13*(1), 128–137. https://doi.org/10.33961/jecst.2021.00780

Rock salt structure. (n.d.). https://www.oxfordreference.com/display/10.1093/oi/authority.20110803100425723

Rubenbauer, H., & Henninger, S. (2017). Definitions and reference values for battery systems in electrical power grids. *Journal of Energy Storage*, *12*, 87–107. https://doi.org/10.1016/j.est.2017.04.004

Saft. (n.d.). *Infographic: Power vs energy* [Accessed: May 15, 2024]. https://saft.com/media-resources/our-stories/infographic-power-vs-energy

Shi, Q., Hu, R., Zeng, M., & Zhu, M. (2010). A diffusion kinetics study of Li-ion in LiV_3O_8 thin film electrode. *Electrochimica Acta*, *55*(22), 6645–6650. https://doi.org/10.1016/j.electacta.2010.06.009

Soult, M. C. (2023). *Cobalt-free electrodes for next generation lithium-ion batteries*.

Soult, M. C., Siller, V., Zhu, X., Gehlhaar, R., Wojcik, P. J., Morata, A., ..., & Hubin, A. (2022). Spectroscopic ellipsometry for operando monitoring of (de) lithiation-induced phenomena on limn2o4 and lini0.5mn1.5o4 electrodes. *Journal of The Electrochemical Society*, *169*(4), 040501. https://doi.org/10.1149/1945-7111/ac5ceb

Springer, T., & Lechner, R. E. (2005). Diffusion in condensed matter. Springer.

Sun, H., Hu, A., Spence, S., Kuai, C., Hou, D., Mu, L., ..., & Lin, F. (2022). Tailoring disordered/ordered phases to revisit the degradation mechanism of high-voltage $LiNi_{0.5}Mn_{1.5}O_4$ spinel cathode materials. *Advanced Functional Materials*, *32*(21). https://doi.org/10.1002/adfm.202112279

Tecate Group. (n.d.). *Ultracapacitor FAQ* [Accessed: April 4, 2024]. https://www.tecategroup.com/products/ultracapacitors/ultracapacitor-FAQ.php#What_is_the_difference_between_power_and_energy

Vieira, F. S., Balestieri, J. A. P., & Matelli, J. A. (2021). Applications of compressed air energy storage in cogeneration systems. *Energy*, *214*, 118904. https://doi.org/10.1016/j.energy.2020.118904

Wang, L., Li, H., Huang, X., & Baudrin, E. (2011). A comparative study of Fd-3m and P4332 "$LiNi_{0.5}Mn_{1.5}O_4$". *Solid State Ionics*, *193*(1), 32–38. https://doi.org/10.1016/j.ssi.2011.04.007

Wanger, T. C. (2011). The lithium future—resources, recycling, and the environment. *Conservation Letters*, 202–206. https://doi.org/10.1111/j.1755-263X.2011.00166.x

Wen, C. J., Boukamp, B. A., Huggins, R. A., & Weppner, W. (1979). Thermodynamic and mass transport properties of "LiAl". *Journal of The Electrochemical Society*, *126*(12), 2258. https://doi.org/10.1149/1.2128939

Weppner, W. R. A. H., & Huggins, R. A. (1977). Determination of the kinetic parameters of mixed-conducting electrodes and application to the system Li_3Sb. *Journal of The Electrochemical Society*, *124*(10), 1569–1977. https://doi.org/10.1149/1.2133112

Winter, M., & Brodd, R. J. (2004). What are batteries, fuel cells, and supercapacitors? *Chemical Reviews*, 4245–4270. https://doi.org/10.1021/cr020730k

Xia, H., Lu, L., & Lai, M. O. (2009). Li diffusion in $LiNi_{0.5}Mn_{0.5}O_2$ thin film electrodes prepared by pulsed laser deposition. *Electrochimica Acta*, *54*(25), 5986–5991. https://doi.org/10.1016/j.electacta.2009.02.071

Xia, H., Meng, Y. S., Lu, L., & Ceder, G. (2007). Electrochemical properties of nonstoichiometric $LiNi_{0.5}Mn_{1.5}O_{4-\delta}$ thin-film electrodes prepared by pulsed laser deposition. *Journal of the Electrochemical Society*, *154*(8), A737. https://doi.org/10.1149/1.2741157

Xia, H., Meng, S. Y., Lu, L., & Ceder, G. (2007). Electrochemical behavior and Li diffusion study of $LiCoO_2$ thin film electrodes prepared by PLD. *Journal of the Electrochemical Society*, *154*(9).

Xie, J., Imanishi, N., Zhang, T., Hirano, A., Takeda, Y., & Yamamoto, O. (2009). Li-ion diffusion kinetics in $LiFePO_4$ thin film prepared by radio frequency magnetron sputtering. *Electrochimica Acta*, *54*(20), 4631–4637. https://doi.org/10.1016/j.electacta.2009.03.007

Xu, B., & Meng, S. (2010). Factors affecting Li mobility in spinel $LiMn_2O_4$—a first-principles study by GGA and GGA+U methods. *Journal of Power Sources*, *195*(15), 4971–4976. https://doi.org/10.1016/j.jpowsour.2010.02.060

Yoshio, M., Brodd, R. J., & Kozawa, A. (2009). *Lithium-ion batteries* (Vol. 1). Springer.

Zhu, Y., & Wang, C. (2010). Galvanostatic intermittent titration technique for phase-transformation electrodes. *The Journal of Physical Chemistry C*, *114*(6), 2830–2841. https://doi.org/10.1021/jp9113333

Zubi, G., Dufo-López, R., Carvalho, M., & Pasaoglu, G. (2018). The lithium-ion battery: State of the art and future perspectives. *Renewable and Sustainable Energy Reviews*, *89*, 292–308. https://doi.org/10.1016/j.rser.2018.03.002